Numerical analysis of the influence of wall thermal inertia on the stability of natural circulation driven supercritical water reactors

Author:
T.K.F. Schenderling 4004752

Supervisor:
Dr.Ir. M. Rohde

Bachelor Thesis

NERA-131-2013-003

Committee:

Dr.Ir. M. Rohde	TNW, TU Delft
Dr.Ir. D. Lathouwers	TNW, TU Delft

Delft University of Technology
Faculty of Applied Sciences
Dept. of Radiation, Science & Technology
Sect. Nuclear Energy & Radiation Applications

Delft,
Wednesday 17th July, 2013

1 Abstract

The Generation IV International Forum have proposed six new nuclear reactor designs. One of these, the SuperCritical Water Reactor (SCWR), which uses supercritical water as its coolant and moderator, is discussed in this thesis. One of the advantages of the SCWR compared to the widely-used Boiling Water Reactor (BWR) is that the thermal efficiency is expected to increase from 33% to 42%.

The European version of the SCWR is the High Performance Light Water Reactor (HPLWR). A model has been built by the section Nuclear Energy and Radiation (NERA) at Delft University of Technology, named the Delft Light water reactor (DeLight).

The DeLight facility mimics the behavior of the HPLWR. It uses Freon R23 as its coolant, which becomes supercritical at lower temperature and pressure than water. The facility was originally built to investigate the stability of the coolant flow when naturally circulating (without pumps). Natural circulation would allow for more inherent safety in the HPLWR, as the core will continue to get cooled when the pumps fail. The stability of DeLight was measured at different core power and coolant inlet temperature settings.

A first computer model by Koopman [2008] for the BWR was adjusted by Kam [2011] for the DeLight and later updated by Spoelstra [2012]. The model is one-dimensional, non-linear and transient.

When Spoelstra compared his results with those of T'Joen and Rohde [2012], who did the measurements on the DeLight, he found that his modeled neutral stability boundary (NSB) was similar to the measurement results at low power over mass flow ratios (a measure for the enthalpy increase in the core section). However, at higher ratios his boundary differed significantly from the measurements, as he found a more unstable system with his model.

The objective of this thesis is to find a possible cause of this difference. Spoelstra [2012] had a constant internal heat flux in the core. In this thesis, the thermal inertia of the core was taken into account as a possible cause of the difference.

After adding thermal inertia to the model, the NSB was recalculated and showed a more stable system over the measured range. At high power over mass flow ratios the agreement with the experiments was improved compared to the results of Spoelstra [2012]. The trend of the measurements at higher power of mass flow ratios seems to have been found. However, at lower ratios the new model predicted a more stable system than the experiments showed.

The Nusselt number for internal heat flux was calculated with a model for subcritical fluids, as opposed to a model for supercritical fluids. Other Nusselt number relations were used as a benchmark. The NSB then changed significantly, showing that it is very dependent on the relation for the Nusselt number. A correct Nusselt number relation should be found to improve on the model.

2 Contents

3 Introduction

3.1 The SCWR

In an attempt to make nuclear reactors even more inherently save, sustainable and proliferation resistant, while keeping them economically attractive, the Generation IV International Forum have proposed six nuclear reactor designs. One of these generation IV reactor designs is the SuperCritical Water Reactor (SCWR). This reactor uses supercritical water as its coolant and moderator. By using supercritical water as opposed to liquid water, a higher operating temperature can be reached than in a non-supercritical reactor, allowing the thermal efficiency of the nuclear reactor to be enhanced. The thermal efficiency of current nuclear reactors like the Boiling Water Reactor (BWR) is approximately 33%. It is estimated that the SCWR can have a higher efficiency of approximately 42%.

Figure 3.1 shows the general design of the SCWR. This design is similar to the design of the widely-used Boiling Water Reactor (BWR). The BWR has already been around for many decades and is therefore proven technology. It operates under lower coolant pressure and temperature, thus not allowing its water to become supercritical.

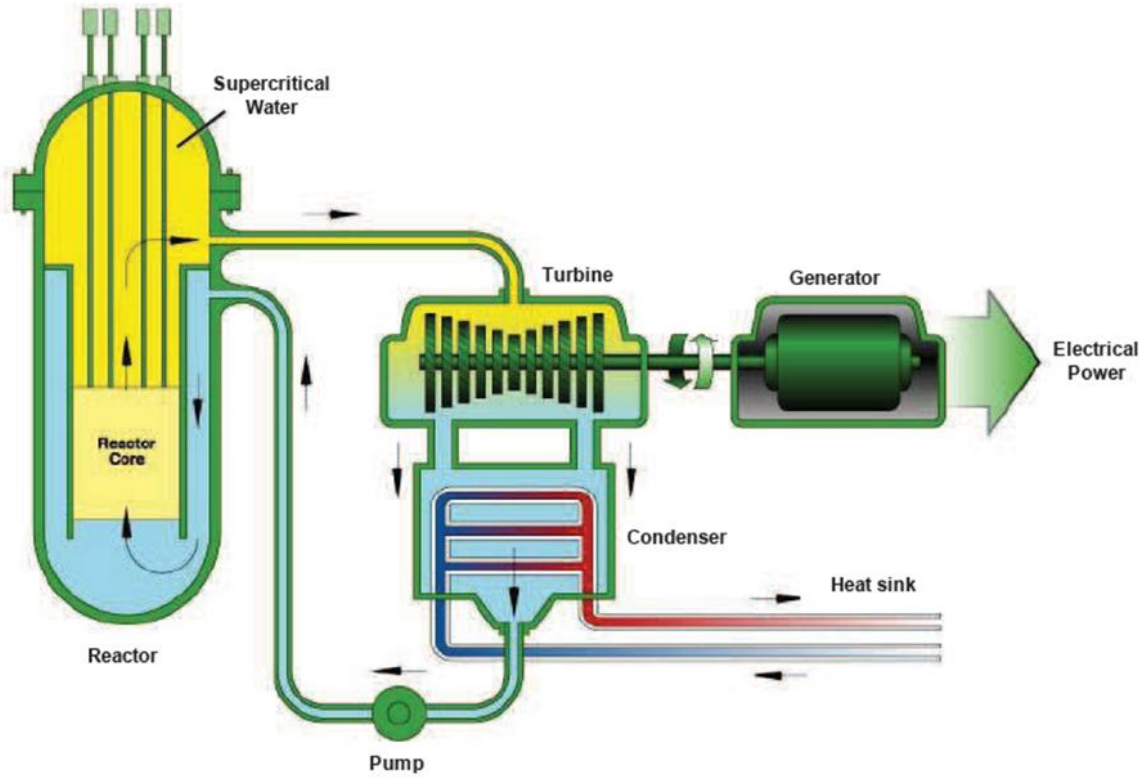

Figure 3.1: General design of a supercritical water reactor. On the left side of this picture, in the reactor, the water goes into the core and is heated. It subsequently goes into the turbine, which drives the generator. The water then goes on to the condenser, cooling it down. Next, it goes through a pump and lastly, it returns to the reactor, making the loop complete. Source: Spoelstra [2012], adjusted.

Besides the BWR, there is also the PWR or the Pressurized Water Reactor. Its operating temperature and pressure are slightly higher than that of the BWR.

In figure 3.2 the three different reactors and their operating pressures and temperatures are shown. It can be seen that the PWR and BWR operate below the critical point. The SCWR operates beyond that point. When a substance has a higher temperature and pressure than at the critical point, it will become supercritical. In the supercritical regime, the separation between the gaseous and the liquid phase of a substance disappears.

For normal fluid-to-gas transitions under the critical point, a liquid will start to boil until all the liquid has changed into gas. It will change its density from high to low. This happens at a single temperature, as all the energy put into the substance will be used for the phase change.

When supercriticality is reached, fluids will not boil anymore, as this would mark a phase change from liquid to gas. The fluids density, however, will still change significantly.

This happens around the so-called pseudocritical point. The pseudocritical point is defined as the point where the heat capacity at constant supercritical pressure is maximal. When a fluid reaches this point, it shows some effects similar to the boiling point for non-supercritical fluids. The boiling itself however, will not take place.

More technical information on supercritical fluids will be discussed in section 4.1.

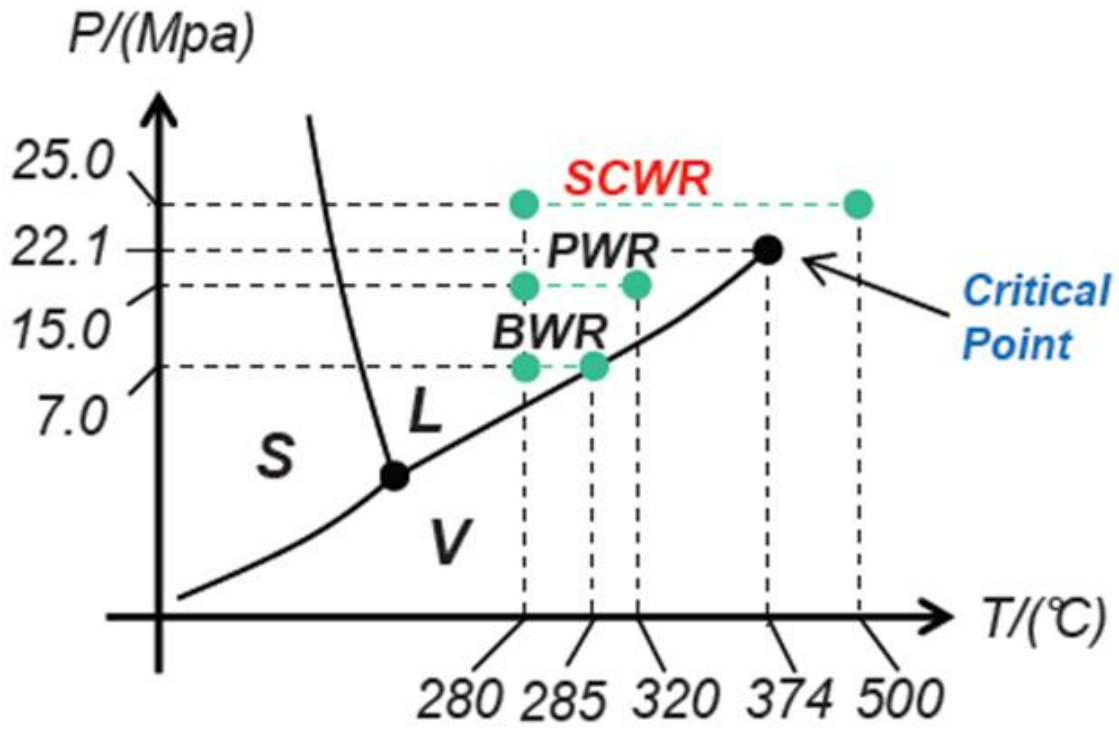

Figure 3.2: Operating temperatures and pressure of the BWR, PWR and SCWR. Source: Spoelstra [2012]

3.2 The HPLWR

Different designs of the SCWR have been made by different countries as part of the Generation IV International Forum. Some examples are the Japanese (SCLWR), American (US-SCWR) and Canadian (CANDUSC) designs. The European version is called High Performance Light Water Reactor (HPLWR). This version has a different core than the other types. It is a triple-pass core; the coolant passes by the core three times. This is done to eliminate hot spots due to the heat deterioration phenomenon (Schulenberg et al. [2008]).

The triple core can be seen in Figure 3.3. The water heats from approximately 310 to 390°C in the first pass. After the second and third pass, the water is 500°C. Water becomes supercritical at temperatures and pressures both above 374°C and 22.1 MPa respectively. As the operating pressure of the system is 25 MPa, the water is supercritical after it leaves the core.

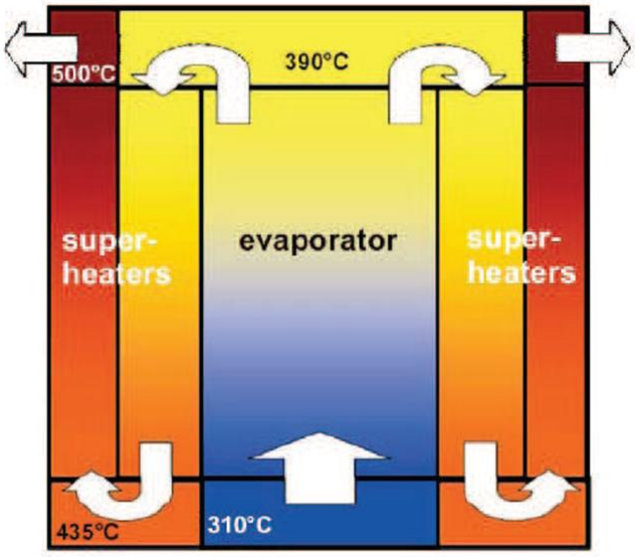

Figure 3.3: The triple core of the HPLWR. Water comes in from the bottom at 310°C. It heats up to 390 degrees and then goes down through Superheater I to attain a temperature of 435 degrees. After Superheater II it has its final, highest temperature of 500°C. Mixing chambers in between core passes mix the water to eliminate hot spots. Source: Spoelstra [2012], adjusted.

It is important to reduce hot spots. The cladding of the HPLWR is designed to be able to withstand temperatures up to 620°C. If the temperature becomes higher, it will have a negative effect on the wall, thus increasing the risk of reactor malfunctions. This can happen when the wall cannot transfer enough heat to the coolant to loose all the heat it produces. In standard operating conditions wall temperatures of 500°C can be reached.

3.3 The DeLight facility

The HPLWR is not yet in development, because more research is needed before it can be implemented as a working nuclear reactor. As one of the goals of the Generation IV

forum is to make the reactors more inherently safe, natural circulation of the coolant can be considered as a way of achieving part of this goal. This type of flow would allow the coolant to go through the system without the use of pumps. This gives the system an advantage over systems with a pump, for example during a power outage. When the pumps in such a system fail, it will become difficult to cool the reactor.

Having natural flow in a reactor also introduces problems. Flow instabilities can occur at a certain power of the core and inlet temperature. This can have a negative effect on the cooling of the reactor. Although a system with pumps can have flow instabilities as well, a system without pumps is more prone to it. To investigate these flow instabilities, a physical model of the HPLWR was made in Delft (Rohde et al. [2011]). This Delft Light water reactor, or DeLight, can be used to investigate flow instabilities in a naturally circulating HPLWR, without using a full-size reactor. The full setup of the delight will be explained in section 4.3

3.4 Previous work

The stability of DeLight was measured by T'Joen and Rohde [2012]. With this measurement he came to a Neutral Stability Boundary (NSB), which is the border between stable and unstable operating points. They found that for a single core inlet temperature there exists a low and high power stability threshold, provided that the N_{SUB} (a dimensionless number, a measure for core inlet temperature) is higher than 0.18. Below this value, no instabilities were recorded.

To see if a relatively simple computer model could reproduce the NSB, a one-dimensional, non-linear, transient model was made by Kam [2011]) , for which he used an existing BWR model by Koopman [2008]. The model by Kam was later updated by Spoelstra [2012].

Spoelstra found, among other things, that results of T'Joen and Rohde [2012] were similar at low power over mass flow ratios, but significantly different at higher ratios. At these higher ratios, the experiments showed a more stable system, while the code predicted less stability (see Figure 3.4).

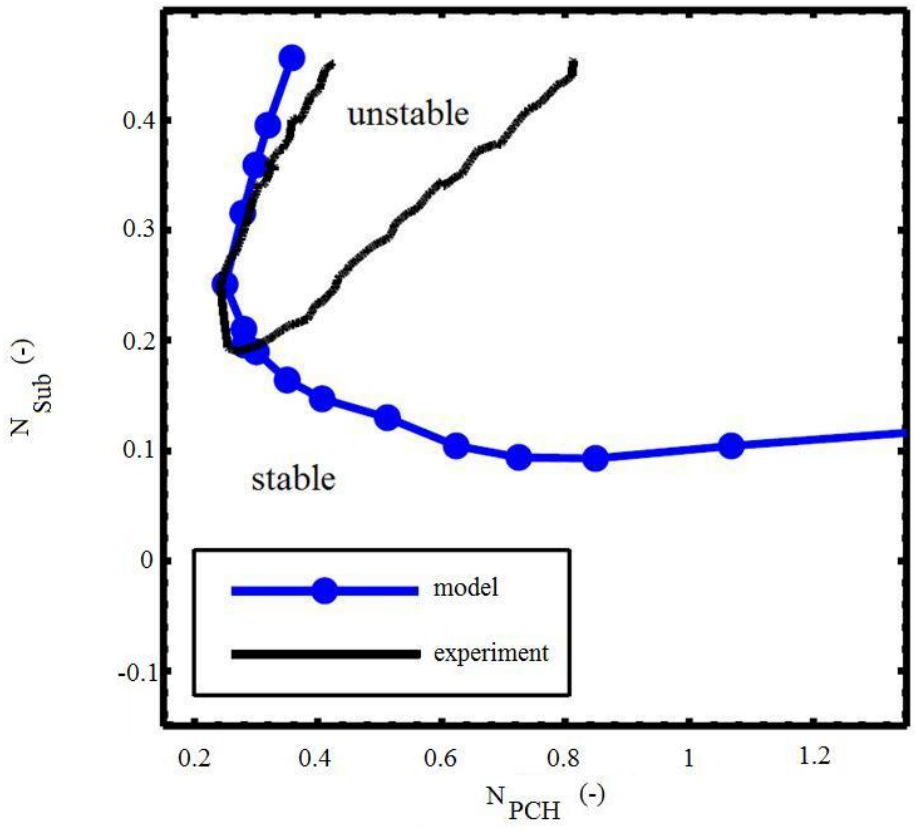

Figure 3.4: The NSBs of the experiment on the DeLight found by T'Joen and Rohde [2012] and the calculated NSB found with the numerical model by Spoelstra [2012]. The dimensionless numbers N_{PCH} and N_{SUB} represent the ratio of power over mass flow rate and core inlet temperature respectively. The exact equations for the dimensionless numbers will be given in section 5.5. Source: Spoelstra [2012], adjusted.

3.5 Thesis objective and outline

The objective of this thesis is to find a possible cause of the difference between the computer model by Spoelstra [2012] and the experiments by T'Joen and Rohde [2012]. It is theorized the modeling of the reactor core added to the difference in NSBs. The computer model by Spoelstra [2012] mimicked a constant amount of heat entering the coolant, while in reality it should be dependent on the thermal properties of the core material. The thermal inertia of the core was thus taken into account.

After implementing the new model into the code, a few benchmarks were first needed to make sure the code was correctly implemented. Afterwards, a new NSB was calculated.

The outline of the thesis is as follows: First, more theory about the DeLight, instabilities and system equations will be discussed in chapter 4. Then, chapter 5 will explain more about the numerical model. Following this, chapter 6 will explain and display the benchmark cases, after which chapter 7 will show the results. Lastly, chapter 8 will show the conclusions and discussion.

4 Theory

4.1 Supercritical fluids

Because the fluid circulating the loop of both the DeLight and the HPLWR is supercritical, it behaves differently than normal liquids or gases. There are some similarities too however. For the setup described in this paper, the differences and similarities of the fluids at the pseudocritical point compared to a subcritical liquid at the boiling point are most important to compare.

When looking at the temperature-density graph of supercritical water in figure 4.1, one can see it is a smooth, decaying curve. This is in contrast to water at a boiling point, where the density would fall suddenly and vertically at the boiling temperature. The similarity here is that both sub- and supercritical water experience a large drop in density in a specific region. This drop in density is a cause for flow instabilities, as discussed in section 4.2.

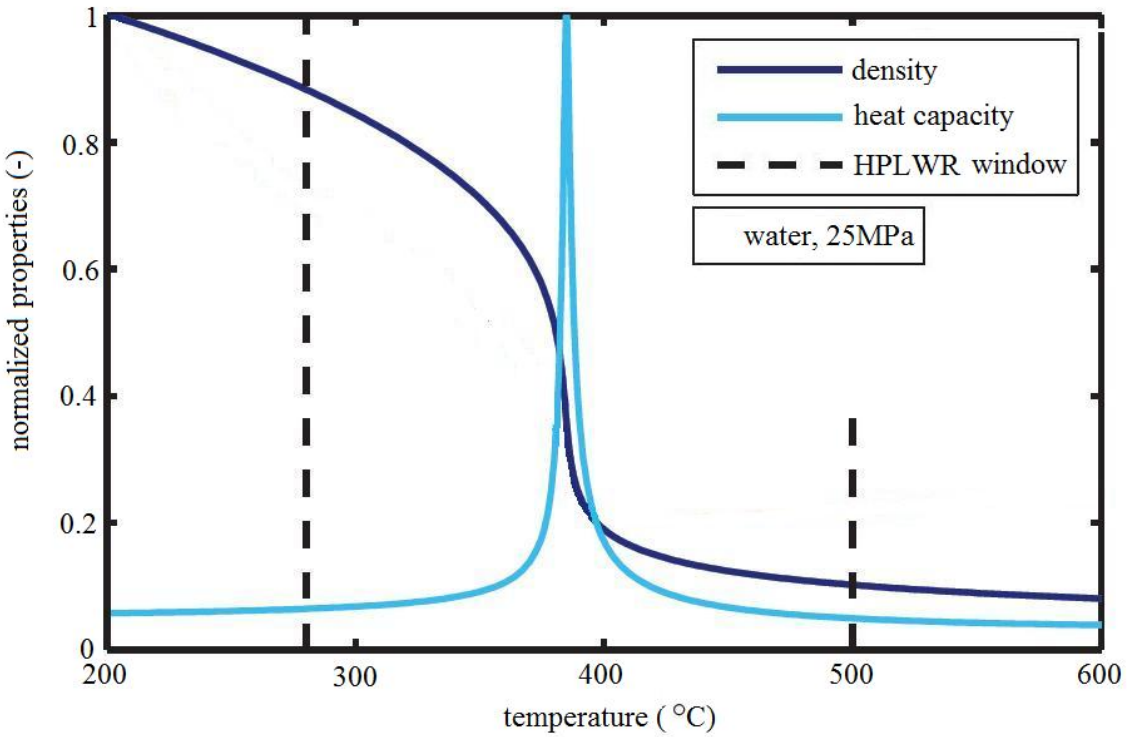

Figure 4.1: Properties of supercritical water near its pseudocritical point at a pressure of 25Mpa, the operating pressure of the HPLWR. The units on the y-axis are normalized. For the density, The value at 200°C is taken as 1. For the heat capacity, the value at the pseudocritical point, 384,90°C is taken as 1. Source: Spoelstra [2012], adjusted.

When looking at the heat capacity of the water, it is clear that there is a certain temperature at which it has the highest value. The pseudocritical point of water is defined at this temperature (T_{pc}), as the point where the heat capacity at constant pressure is maximal. At 25 MPa, this point would be 384,90°C. This is the point where

the enthalpy of the water steeply increases and therefore the derivative of enthalpy with respect to the temperature is the highest: $(dh/dT) = C_p(T_{pc})$ at constant pressure and chemical potential.

When comparing the heat capacity as we have compared the density, there is one noticeable difference. The heat capacity of a subcritical fluid becomes infinite at the boiling point. This is because (dh/dT) is infinite, as the temperature does not rise here, while the enthalpy does. Since the enthalpy rises at constant temperature (the fluid expands, but does not increase its temperature), a clear 'boiling enthalpy' does not exist; it happens at an enthalpy range. A clear pseudocritical enthalpy does exist however, as all temperatures around the pseudocritical point have their own distinctive enthalpy associated with them.

The Delight uses supercritical Freon-R23 as its cooling fluid and the HPLWR uses supercritical water. The following table, table 4.1 gives the pseudocritical temperatures and pressures of Freon and water at operating pressures of the DeLight and HPLWR respectively.

Table 4.1: pseudocriticalv and critical enthalpy and temperature for Freon and water at operating pressure

	Freon R23	**water**
critical pressure (MPa)	4.83	22.06
critical temperature (°C)	26.14	373.95
operating pressure (MPa)	5.70	25.00
$h_{pc}\left(\frac{J}{kgK}\right)$	288.33	2152.90
T_{pc} (°C)	33.22	373.95

4.2 Instabilities

Flow instabilities (see figure 4.2) are an inherent part of natural convection circulating systems. A lot of effort has gone into studying these instabilities in the past, which has resulted in a good understanding of the phenomena. This effort however, focused mostly on the subcritical regime. In current nuclear reactors, the coolant must boil to power the generator. The large density difference at the boiling point causes several types of instability. As supercritical water does not boil when reaching the pseudocritical point, the knowledge of the instabilities is not directly applicable to the natural circulating loop discussed in this thesis. Nevertheless, a large density change related to boiling can also be found when a supercritical fluid passes the pseudocritical point, even though the change is more gradual. Because some instabilities that occur in boiling systems are associated with the large density change, a supercritical fluid loop passing the pseudocritical point is expected to experience these instabilities as well (Gomez [2009])

Flow instabilities are undesirable when operating a nuclear reactor. They can degrade system control and can cause unsafe operating conditions. Water traveling through the core too slowly will heat up too much and have a negative effect on the

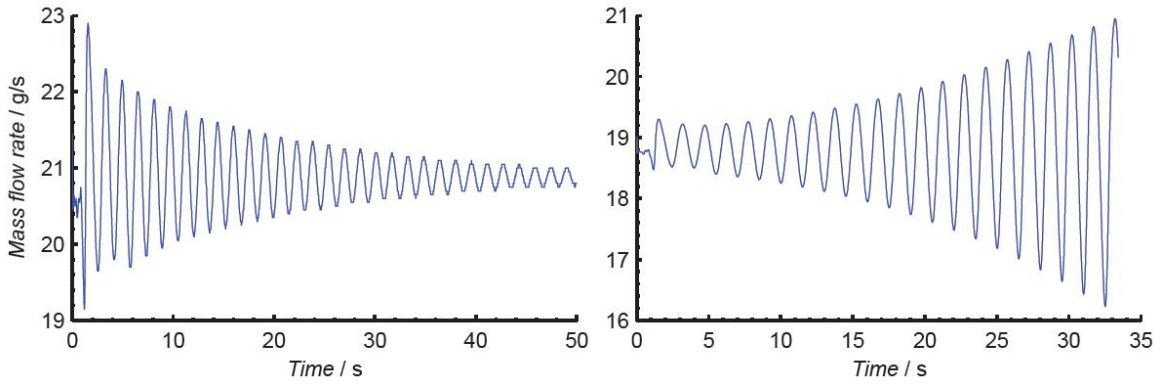

Figure 4.2: Examples of stable (left) and unstable (right) operating conditions. Source: Spoelstra [2012]

wall, as the wall cannot transfer enough of its heat to the water. Water traveling too fast may not reach the pseudocritical point and will diminish the thermal efficiency. Moreover, if a positive feedback loop is present it will further diminish control of the system.

To give an order to the different types of flow instabilities, the classification system by Boure et al. [1973] will be used. Boure makes a distinction between two major types of instability: static and dynamic.

The mechanism of static instabilities can be explained by steady-state characteristics of the thermal-hydraulic system. They can be predicted by analysis of the pressure drop and flow rate characteristics of the channel.

Dynamic instabilities is positive feedback due to inertia. Dynamic instabilities cannot be predicted by simple analysis of the steady-state solution and must be found by looking at the time-dependency of the system.

Some possible causes for instabilities in the DeLight-setup will be discussed in this section. These include Ledinegg instability, density wave oscillations and instabilities caused by the coupling of neutronics and density.

4.2.1 Ledinegg instability

Ledinegg instability is an example of a static instability. It is often associated with the loops that include pumps, but appear in natural circulation loops as well. Ledinegg flow instability occurs when multiple flow rates are possible at the same core pressure drop. When these multiple flow rates are possible, a small perturbation in the flow can result in a wholly different steady-state flow rate. As stated before, a slower flow rate might heat up the coolant too much. A faster flow rate could deteriorate the thermal efficiency. This type of instability is not studied in this paper. Boure et al. [1973]

4.2.2 Density wave oscillations

A different type of flow instability is the Density Wave Oscillation or DWO, which is a dynamic type of instability. This kind of behavior is most common in two-phase flow, like in the BWR, due to the sudden density drop at the boiling point. Although

the HPLWR does not exhibit two-phase flow, the density change at the pseudocritical point is high and therefore DWOs are expected to occur in the DeLight (Gomez [2009] and T'Joen and Rohde [2012]).

There are two types of density wave oscillations discussed in this paper (Fukuda and Kobori [1979]). Type I manifests itself over the length of the core and riser, while type II takes place in the core alone. Due to the fact that type I is placed over a greater length, its frequency is lower than that of type II.

Both types of DWO instability start with a small sinusoidal perturbation of the flow, which are quite common. The slower part of the flow will have more time to pick up heat from the core and by the end of the core it will be a bit warmer than the fast part. In case the pseudocritical point of the coolant is reached around the top of the core, the slow part will have a noticeably lower density here than the fast part. This results in a density wave oscillation going through the loop, affecting the system.

Type I instability occurs when the core inlet mass flow and riser gravitational pressure drop oscillations, induced by the DWO, are 180° out of phase. That means a decrease in flow, thus a lower density at the end of the core, results in an increase in riser pressure drop. This allows for positive feedback, increasing instability.

Type II is created when the inlet flow and frictional pressure drop over the core are 180° out of phase (see figure 4.3). The density wave oscillation traveling through the core becomes larger in amplitude as it absorbs more heat. The local pressure drop oscillates with it. The total channel pressure drop is then found by integrating over the local pressure drops, which can result in an increasing inlet flow and a decreasing core pressure drop at the same time. This again can cause positve feedback and thus instability.

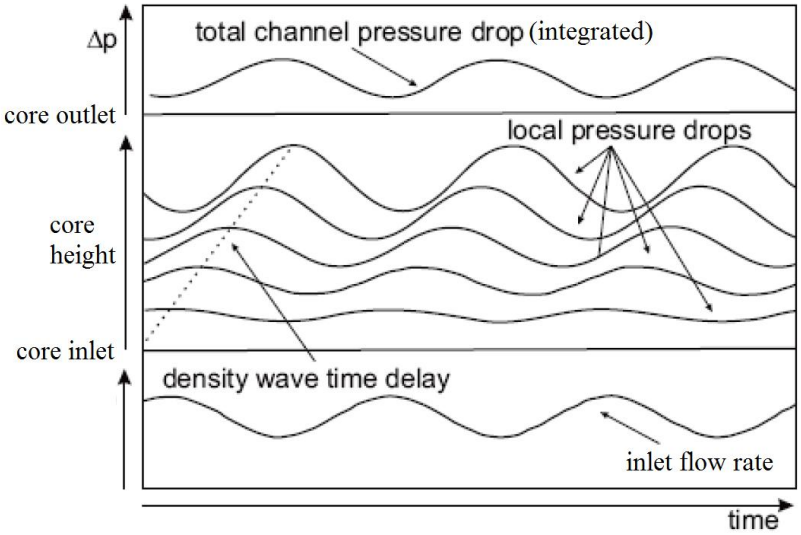

Figure 4.3: Density wave oscillation in the reactor core resulting in type II instability. One can see that the total channel pressure drop and the inlet flow rate are 180° out of phase. Source: Gomez [2009], adjusted

4.2.3 Coupling of neutronics and density

The last type of instability discussed here is due to the coupling between coolant density and core neutronics. Because the coolant in a HPLWR acts as a moderator as well, a higher coolant density causes higher reactor power and vice-versa. Oscillations in the density of the coolant present in the core can therefore cause fluctuation in the reactor output power. This in turn affects the density of the coolant. This feedback loop is not instantaneous; fission energy released in the fuel rods takes time to transport through the core wall to the coolant. Therefore, a positive feedback may occur, leading to unstable behavior.

4.3 Setup of the DeLight

The setup of the DeLight facility can be seen in Figure 4.4. This setup was used by T'Joen and Rohde [2012] to measure the DeLight's stability. The triple core is in the bottom left of the figure. It is divided into three sections: the evaporator, superheater 1 and superheater 2. The core is heated by sending an electric current through the stainless-steel core wall. This creates a constant power output throughout a section of the core wall, meaning a constant amount of heat is created throughout that section. The total electrical power created, which will be to be transformed into heat in the core wall, will be distributed amongst the three different sections.

The core neutronics of the HPLWR are artificially recreated in the DeLight. The time needed for the feedback is introduced as an adjustable time constant τ, which in this thesis was always set as 6 seconds.

In stable operating conditions, the coolant flow through the system is clockwise. The part of the loop between the looking glass and the temperature sensor is therefore called the riser and the part of the loop after the buffer is called the downcomer. The density of the coolant, Freon R23, is lower after the core heats it up. After the heat exchangers (SWEP HX and Vahterus HX), the Freon cools down and has a higher density again. The density of the coolant in the riser is therefore lower than the density of the coolant in the downcomer. For this reason gravity allows natural flow in the system in the clockwise direction.

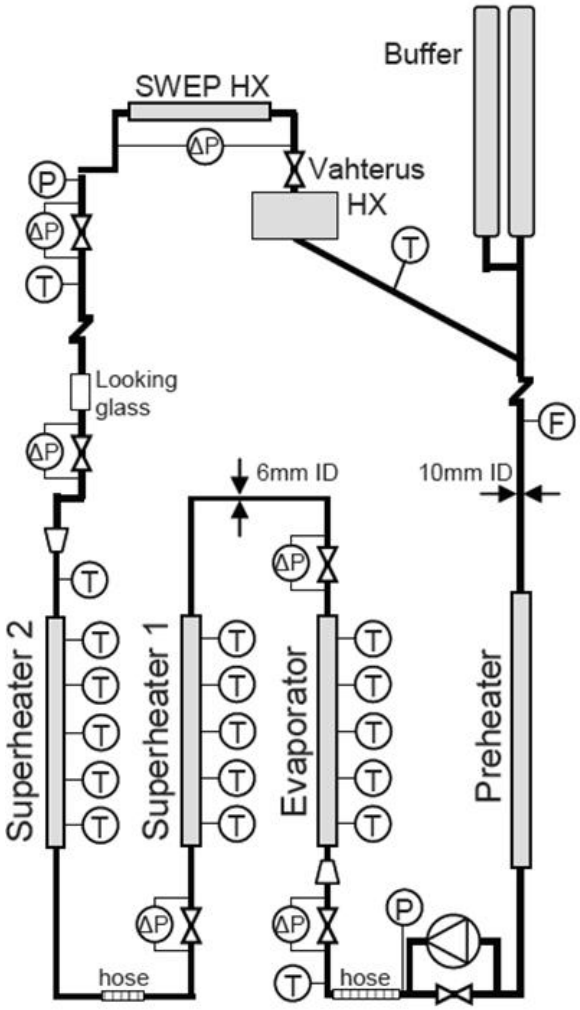

Figure 4.4: A schematic drawing of the setup of the DeLight. The triple core, consisting of the evaporator, superheater 1 and superheater 2, can be seen on the bottom left. From here, the supercritical Freon goes up through the riser, then through two heat exchangers (SWEP HX and Vahterus HX), past the buffer vessel and back down via the downcomer to the preheater. Between the preheater and the triple core, there is a pump, which can be bypassed. The two 'zigzags' found in the loop indicate a leap in distance. They can be replaced by the riser on the left and the downcomer on the right. The riser and downcomer are long, vertical parts of the loop, meant to stimulate natural flow. Temperature, pressure and pressure drop indicators are shown with a T, P and ΔP respectively. Source: Spoelstra [2012].

4.4 Thermal inertia

4.4.1 Effect of thermal inertia

In the previous computer model by Spoelstra [2012], the heat transfer in the DeLight core was implemented by a constant amount of heat per second going from the core wall into the coolant over an entire core section. That is, each of the three parts (evaporator, superheater 1 and superheater 2) of the triple core was set to a specific

power. The linear heat flux from the wall into the Freon was calculated by using

$$Q' = p_{tot} \frac{P_{core} \frac{1 - p_{loss}}{100}}{L_{core}}. \tag{4.4.1}$$

Here, Q' is the linear heat flux, P_{core} is the amount of heat produced in the entire triple core per second, p_{tot} determines the distribution of that heat production over the core bypasses in percentages, p_{loss} is the percentage of heat lost to the environment and L_{core} is the length of a single part of the core.

The use of this equation is correct when the heat flux to the coolant is constant. However, it is expected that this is not the case. Heat transfer is dependent on temperature difference. The temperature of the coolant at the start of the core is considerably lower than at the end. To have any heat transfer from the wall into the coolant, the core wall must be hotter than the coolant.

Heat transfer to the environment is also dependent on the temperature difference. Because the environmental temperature at a distance is assumed to be constant at 23°C, the temperature difference here rises linearly with the wall temperature.

Therefore, when you go further along the core, relatively more heat will be transferred to the environment than at the start of the core. In other words, more heat will go into the coolant at the start of the core than at the end.

For the internal heat flux, If one would, for the sake of simplicity, assume a constant wall temperature, then the temperature difference of the wall and the coolant is solely dependent on the temperature of the coolant. The higher the temperature difference of the wall and the Freon, the higher the heat transfer. Or as the Freon temperature rises, the heat transfer deteriorates.

The above mechanism has an effect on stability. When a perturbation occurs, a coolant temperature oscillation will enter the core. The cold part of the oscillation will receive more heat per second from the wall than the warm part. This means the cold part will heat up faster than the warm part and thus the oscillation dampens. But this is only true when assuming constant wall temperature and Nusselt number. The heat transfer to the ambient air is constant here, as the temperature difference between the wall and the ambient air is constant.

The above case occurs when the heat capacity, density and/or the volume of the wall are infinite. In reality there are more aspects to take into account. First of all, the wall temperature will be significantly lower at the start of the core, where the Freon is cold, than at the top, where the Freon has heated up as well. Second, the heat transfer to the environment starts to become a function of the place in the core, as the temperature difference at the top of the core will be higher than at the bottom. However, this situation is still expected to dampen the oscillation; The warm part of an oscillation will cause the core to heat up slightly, whereas the cold part will take the stored energy away, thus heating up faster. The amount of heat taken from the core wall is still dependent on the temperature difference between the Freon and the wall.

Third, the Nusselt number is not a constant, hence it becomes even harder to predict whether this mechanism will have a dampening effect. As the Nusselt number is dependent on several aspects of the Freon, warmer Freon might cause a higher Nusselt

number, thereby absorbing more heat from the wall. This might have a stronger effect than the temperature difference effect and because of that, the system might become more unstable instead of stable.

4.4.2 Thermal inertia model

In an attempt to better approximate the influence of the wall temperature, a different equation was used to calculate the heat transfer to the Freon per second:

$$\rho C_p V \frac{dT_{wall}}{dt} = Q - \alpha_{in} \left(T_{wall} - T_{Freon}\right) P_{in} dz - \alpha_{out} \left(T_{wall} - T_{ambient}\right) P_{out} dz. \quad (4.4.2)$$

Here, ρ and C_p are the density and specific heat capacity of the wall respectively, V is the volume of the wall over a length dz, T_{wall} is the temperature of the wall, Q is the power produced in the core wall, α_{in} and α_{out} are the heat transfer coefficients to the Freon and to the air respectively, T_{Freon} is the temperature of the bulk of Freon, $T_{ambient}$ is the temperature of the ambient air at a large distance, P_{in} is the perimeter of the inner part of the core wall and P_{out} is the perimeter of the outside of the core wall.

This equation can be verified by understanding where the heat created in the core wall goes. The first part of this equation signifies the amount of heat stored in the core wall. The second part, Q, gives the amount of heat created in the core wall, the thermal inertia. The third and fourth part calculate the heat going into the Freon and out to the air respectively. Furthermore, one can see that the axial heat conduction was not taken into account. This is to keep the equation, and therefore the project, as simple as possible, while keeping physical meaning.

In equation 4.4.2 the heat transfer to the Freon and to the air is dependent on temperature difference. However, the heat transfer coefficients α_{in} and α_{out} are not immediately found in literature. They have to be approximated using the following equations:

$$\alpha_{in}(z) = Nu_{in}(z) \frac{\lambda_{Freon}}{D_H} \quad (4.4.3)$$

and

$$\alpha_{out}(z) = Nu_{out}(z) \frac{\lambda_{air}}{D}. \quad (4.4.4)$$

Here, Nu_{in} is the Nusselt number for forced convection by turbulent flow in pipes, λ_{Freon} is the thermal conductivity of the bulk fluid and D_H is the hydraulic diameter, Nu_{out} is the Nusselt number for natural convection outside vertical cylinders, λ_{air} is the thermal conductivity of air and D is the diameter of the outside of the core wall.

Using these equations, the values must be found for both of the Nusselt numbers. Using the Dittus-Boelter equation (Janssen and Warmoeskerken [1987]), the Nusselt number for forced convection by turbulent flow in pipes is

$$Nu_{in}(z) = 0.027 Re_z^{0.8} Pr_{in}^{0.3333} \quad (4.4.5)$$

and the Nusselt equation for natural convection outside vertical cylinders is found with the Le Fevre and Ede (1956) equation:

$$Nu_{out}(z) = \frac{4}{3}\left(\frac{7GrPr_{out}^2}{5\left(20+21Pr_{out}\right)}\right)^{\frac{1}{4}} + \frac{4\left(272+315Pr_{out}\right)L}{35\left(64+63Pr_{out}\right)D}, \tag{4.4.6}$$

where Re is the Reynolds number of the Freon flow in the core, Pr_{in} is the molecular Prandtl number of the Freon, Gr is the Grashof number of air, Pr_{out} is the Prandtl number of air, L is the length of the core and D is the outer diameter of the core.

The Grashof number is defined as

$$Gr = \frac{g\beta\left(T_{wall}-T_{amb}\right)D^3}{\nu^2}, \tag{4.4.7}$$

where g is the acceleration due to gravity, β is the volumetric thermal expansion coefficient and ν is the kinematic viscosity.

the ambient air was taken as an ideal gas and therefore β can be written as $(1/T_{avg})$, where T_{avg} is the temperature average of the wall temperature and the ambient temperature.

Using these equations, one can find the theoretical wall temperature of the core with equation 4.4.2. When that is found, the amount of heat going from the core to the Freon and to the air can be obtained by

$$Q'_{in}(z) = \alpha_{in}(z)\left(T_{wall}-T_{Freon}\right)Per_{in} \tag{4.4.8}$$

and

$$Q'_{out}(z) = \alpha_{out}(z)\left(T_{wall}-T_{ambient}\right)Per_{out} \tag{4.4.9}$$

Here, Q'_{in} is the power going from the wall into the Freon, Q'_{out} is the heat transfer from the wall to the air, Per_{out} is the inner perimeter of the core wall and Per_{in} is the outer perimeter of the core wall.

Together, Equations 4.4.2-4.4.9 can replace Equation 4.4.1 in the computer model for the heat transfer between the core, the Freon and the ambient air.

4.4.3 Changing the model of the Nusselt number

Several benchmark cases were done in this thesis (chapter 6), these include steady state benchmarks and stability benchmarks. In an attempt to study the effect of the Nusselt number on stability, the model for the Nusselt number was changed. Two models were chosen, both found in Pioro and Mokry [2011]. The first is the model by Bishop et al., made in 1964, who investigated supercritical water flowing upward inside bare tubes and annuli. This resulted in the following model:

$$Nu_B = 0.0069Re^{0.9}Pr^{0.66}\left(\frac{\rho_w}{\rho_b}\right)^{0.43}\left(1+2.4\frac{D}{x}\right) \tag{4.4.10}$$

where Nu_B is the Nusselt number by Bishop, ρ_w is the density of the fluid close to the wall, taken as the density when the fluid would have the temperature of the wall,

ρ_b is the bulk density of the fluid, D is the diameter of the wall and x the distance in the wall.

The last term, $\left(1 + 2.4\frac{D}{x}\right)$, has been dropped, as this accounts for entrance region effects, which are not taken into account in this thesis.

The second model was made by Jackson et al. in 2002. It is the following equation:

$$Nu_J = 0.0183 Re^{0.82} Pr^{0.5} \left(\frac{\rho_w}{\rho_b}\right)^{0.3} \left(\frac{\bar{C_p}}{C_{pb}}\right)^n \tag{4.4.11}$$

where Nu_J is the Nusselt number by Jackson, $\bar{C_p}$ is the averaged specific heat capacity within the range of $(T_w - T_b)$. It is given by $\left(\frac{H_w - H_b}{T_w - T_b}\right)$, C_{pb} is the specific heat capacity of the bulk and lastly, n is given by:

$n = 0.4$ for $T_b < T_w < T_{pc}$ and for $1.2T_{pc} < T_b < T_w$,

$n = 0.4 + 0.2\left(\frac{T_w}{T_{pc}} - 1\right)$ for $T_b < T_{pc} < T_w$ and

$n = 0.4 + 0.2\left(\frac{T_w}{T_{pc}} - 1\right)\left[1 - 5\left(\frac{T_w}{T_{pc}} - 1\right)\right]$ for $T_{pc} < T_b < 1.2T_{pc}$ and for $T_b < T_w$

These two equations have replaced the Dittus-Boelter equation in the code for this benchmark.

5 Numerical model

5.1 Semi-implicit scheme

In this chapter, a small overview is given of the numerical model. For the full description, please see the description of the model in Spoelstra [2012].

The numerical model implemented in the computational code by Spoelstra [2012] makes use of a combination of an forward Euler scheme and a backward Euler scheme. The forward Euler scheme, which is explicit, is accurate and computationally cheap per time step. However, it requires sufficiently small time steps to be stable, which increases the computational costs. The backward Euler scheme, which is implicit, is unconditionally stable, even at larger time steps, but is computationally demanding and less accurate.

The combination of both these schemes is called the semi-implicit scheme. It makes use of the variable θ that indicates which of the two schemes is the most influential in finding the solution to the differential equation under observation. The value of θ can be set anywhere between 1 and 0. When θ is 1, only the explicit forward scheme is used, when θ is 0, only the implicit backward scheme is used. Any value in between 0 and 1 makes use of both schemes. In this research, θ was set to 0.6 Bijl [1999].

5.2 Indexing

In order to prevent odd-even decoupling of the pressure field (Patankar [1980]), the model makes use of a staggered grid (Figure 5.1). The position indexes are i and j. Position i is where the momentum balance is integrated. Position j is where the mass and enthalpy balance are integrated. Every cell has size Δx and therefore $j+1$ is Δx further along the modeled system than j. The same applies to i and $i+1$.

When all variables have been found for all cells in one time step n, the system goes to the next time step $n+1$, which is an amount of time Δt later.

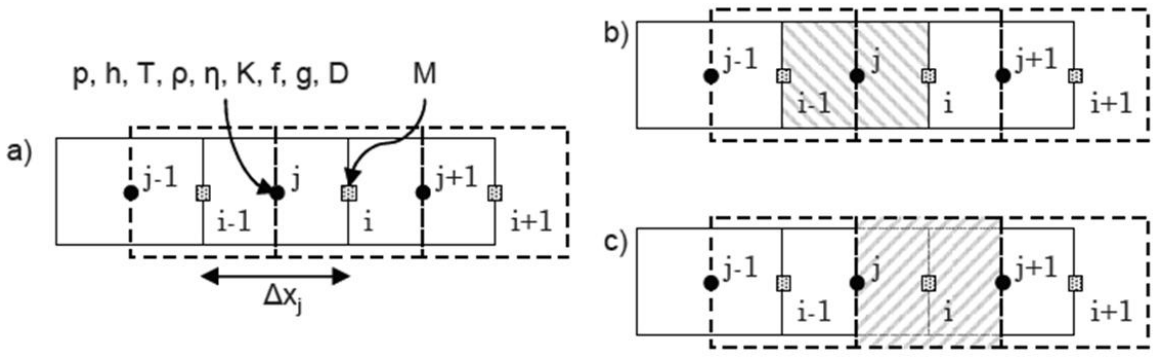

Figure 5.1: a) control volume definitions for the staggered grid, b) the mass and enthalpy balance for index j, c) the momentum equation for index i. Source: Spoelstra [2012].

5.3 Discretization of the wall temperature equation

To use the balance equations in a computer model, one needs to discretize them. Discretization of the balance equations for the computer model has been done by Spoelstra and will not be shown here. However, equation 4.4.2, that is to say

$$\rho C_p V \frac{dT_{wall}}{dt} = Q - \alpha_{in} \left(T_{wall} - T_{Freon}\right) P_{in} dz - \alpha_{out} \left(T_{wall} - T_{ambient}\right) P_{out} dz.$$

is new to the model and when discretized using the grid indices from the previous section and supplying an explicit scheme,

$$\begin{aligned} &\rho_i C_{p,i} V_i \frac{T^{n+1}_{wall,i} - T^n_{wall,i}}{\Delta t} = \\ &Q^n_i - \alpha^n_{in,i} \left(T^n_{wall,i} - T^n_{Freon,i}\right) P_{in,i} dx_{set} - \alpha^n_{out,i} \left(T^n_{wall,i} - T_{ambient}\right) P_{out,i} dx_{set}. \end{aligned} \tag{5.3.1}$$

Where the position indexes i is a subscript and the time index n is a superscript. dx_{set} is the step size for the descretization. As can be seen, the parameters from previous time step are used to find the parameter of the next time step.

Using an implicit scheme, the equation to find the core wall temperature is:

$$\begin{aligned} &\rho_i C_{p,i} V_i \frac{T^{n+1}_{wall,i} - T^n_{wall,i}}{\Delta t} = \\ &Q^{n+1}_i - \alpha^{n+1}_{in,i} \left(T^{n+1}_{wall,i} - T^{n+1}_{Freon,i}\right) P_{in,i} dx_{set} - \alpha^{n+1}_{out,i} \left(T^{n+1}_{wall,i} - T_{ambient}\right) P_{out,i} dx_{set}, \end{aligned} \tag{5.3.2}$$

where the time stepping parameter n was replaced by $n+1$ in the right side of the equation. Now the wall temperature is detemined with the parameters from the current time step in stead of those from the previous one. These current parameters have been readily determined in the code and are therefore known. Because $T^{n+1}_{wall,i}$ is now implicitly determined, it must be found by matrix calculation. How this is done can be found in Spoelstra [2012].

Combining these two equations to make the semi-implicit scheme, gives the following equation:

$$\begin{aligned} &\rho_i C_{p,i} V_i \frac{T^{n+1}_{wall,i} - T^n_{wall,i}}{\Delta t} = \\ &\theta Q^{n+1}_i - \theta \alpha^{n+1}_{in,i} \left(T^{n+1}_{wall,i} - T^{n+1}_{Freon,i}\right) P_{in,i} dx_{set} - \theta \alpha^{n+1}_{out,i} \left(T^{n+1}_{wall,i} - T_{ambient}\right) P_{out,i} dx_{set} \\ &+ (1-\theta) Q^n_i - (1-\theta) \alpha^n_{in,i} \left(T^n_{wall,i} - T^n_{Freon,i}\right) P_{in,i} dx_{set} \\ &- (1-\theta) \alpha^n_{out,i} \left(T^n_{wall,i} - T_{ambient}\right) P_{out,i} dx_{set}. \end{aligned} \tag{5.3.3}$$

Where θ, as indicated before, defines the influence of the implicit scheme compared to the explicit scheme on a scale of 0 to 1.

5.4 Model description

The wall temperature mechanism uses several parameters calculated in the code by Spoelstra. For this reason, it was decided that the wall temperature would be calculated at the end of each time step. The updated wall temperature mechanism variables are then used as input for the wall temperature code and so on. The exact position of the new code in the loop can be found in bold print in figure 5.3.

The code is run for a set of points on the non-dimensional plane described in section 5.5. The procedure for running the code contains two main parts. First, the steady state conditions per point are calculated by running the code with a relatively large spatial step and large temporal step (20mm and 1s respectively). These spatial and temporal steps are usually too large to accurately detemine instabilities, which is why the code is run again afterwards. In this second run, the conditions are copied from the end of the first run, but the spatial and temporal steps are decreased. These have become 10mm and 2.5ms respectively, small enough to find instabilities. These values were originally used by Spoelstra [2012]. As a benchmark case, the spatial and temporal steps have been decreased further and this showed no significant change in the value of the decay ratio or the frequency. It is concluded that the original spatial and temporal time step sizes were indeed small enough and the results were not influenced by the size of the steps.

Due to startup problems with the first part of the procedure, the code commenced with the code by Spoelstra [2012] instead of the code with the wall temperature mechanics included. The influence of the wall is then switched on halfway through the startup, after which the code adjusted to the mechanics and changed its operating conditions accordingly.

To make the neutral stability boundary, multiple points in the stability plane were measured. Afterward, the decay ratios of all points were analyzed. The NSB is the result of interpolating between two neighboring points, one of which has a decay ratio larger than 1 and the other smaller than 1.

5.5 Stability analysis

The stability analyses resulted in a Neutral Stability Boundary. This NSB was set in a non-dimensional plane consisting of a pseudo-phase change number (N_{PCH}) on the x-axis and a pseudo-subcooling number (N_{SUB}) on the y-axis. These dimensionless numbers can be found in T'Joen and Rohde [2012]. They are defined as:

$$N_{PCH} = \frac{P_{core}}{M h_{pc}} \tag{5.5.1}$$

$$N_{SUB} = \frac{h_{pc} - h_{in}}{h_{pc}} \tag{5.5.2}$$

where P_{core} is the core power, M is the mass flow rate, h_{pc} is the enthalpy at the pseudocritical point of the Freon at 5.70MPa and h_{in} is the enthalpy at which the Freon enters the core. The value of h_{pc} is set at $288.33 \frac{J}{kgK}$ See table 4.1 for the value of h_{pc}.

Thus the y-axis is only dependent on the enthalpy at which the Freon enters the core. The x-axis, however is dependent on two variables: P_{core} and M, together making the x-axis dependent on the enthalpy added in the core. In a natural circulation loop, the mass flow rate is determined by the core power. The relation looks as in figure 5.2.

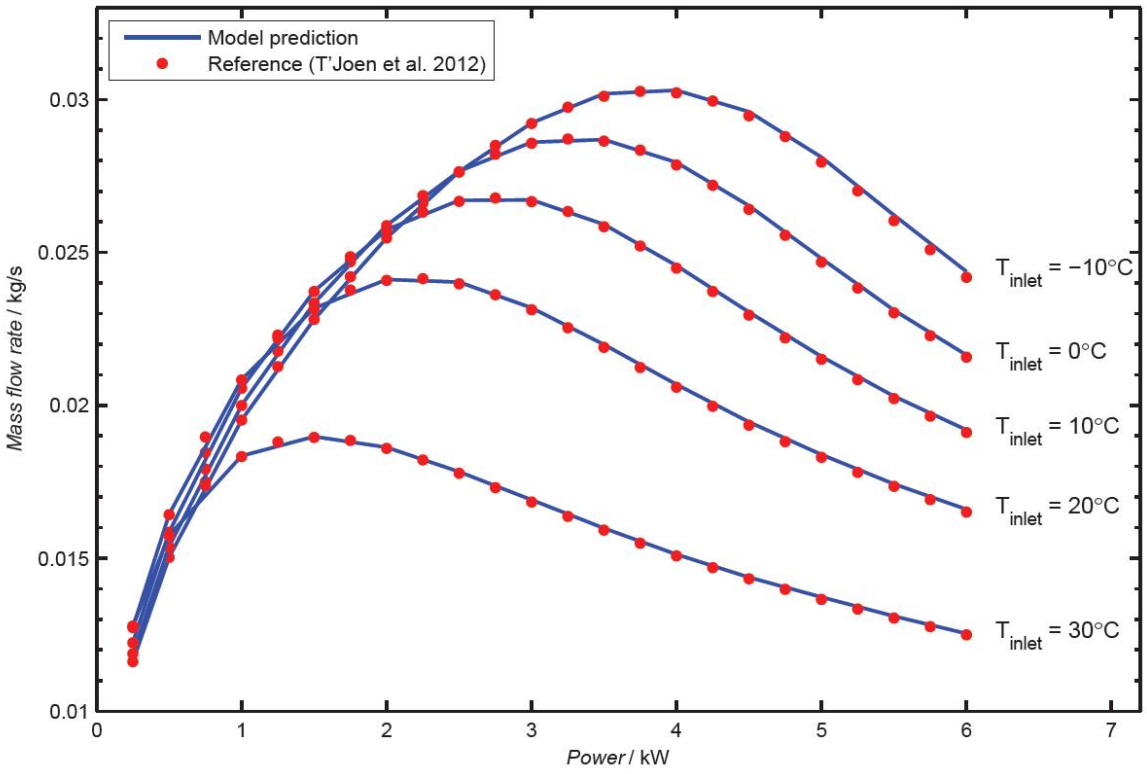

Figure 5.2: The predicted power flow maps at several core inlet temperatures by Spoelstra. These were matched against the measured values by T'Joen. The results were matched within a 1% relative error. Note that these lines will have changed due to adding the code for the wall temperature. Source: Spoelstra [2012]

5.5.1 Autocorrelation and decay ratio

The examples of stable and unstable responses to perturbations given in figure 4.2 can be seen as a combination of cosine and exponential functions. As such, they can be described as a function consisting of these parameters. This is used to fit an autocorrelation function over the line and thereby giving the possibility to find the frequency and the so-called decay ratio of this autocorrelation function. Although this example shows mass flow oscillation, the oscillation can be observed in all flow variables (flow rate, enthalpy, density and pressure). The variable chosen by T'Joen and Rohde [2012] was the core outlet coolant temperature. The outlet temperature is fitted for multiple frequencies. In case of three frequencies this looks as follows:

$$y = a_0 + \left(1 - a_0 - \sum_{i=2}^{4} a_i\right) e^{b_i t} + \sum_{i=2}^{4} a_i e^{b_i t} \cos \omega_i t. \tag{5.5.3}$$

The decay ratio and the frequency are then found by using

$$DR_i = e^{\frac{2\pi b_i}{|\omega_i|}} \tag{5.5.4}$$

$$f_i = \frac{|\omega_i|}{2\pi}, \tag{5.5.5}$$

where the frequency of the oscillation f is found by finding the main frequency using the power spectral density function. DR stands for the decay ratio, which is a measure for the instability of the system. When the decay ratio is smaller than 1, the system is stable and an oscillation caused by a perturbation will dampen. When the decay ratio is larger than 1, a small perturbation will grow and cause the system to become unstable. Lastly, a decay ratio of exactly 1 will cause a perturbation to neither dampen nor grow. It will stay constant.

As a system should be in safe operating conditions, the decay ratio should always be significantly smaller than one. For this thesis however, the border between stable and unstable operating conditions is sought for. This border, where the decay ratio is equal to 1, is called the Neutral Stability Boundary, or the NSB.

The non-linear fit of equation 5.5.3 is made using the *nlinfit.m* function from the Matlab function database. The power spectral density is obtained by Fourier transforming the signal with *fft.m*.

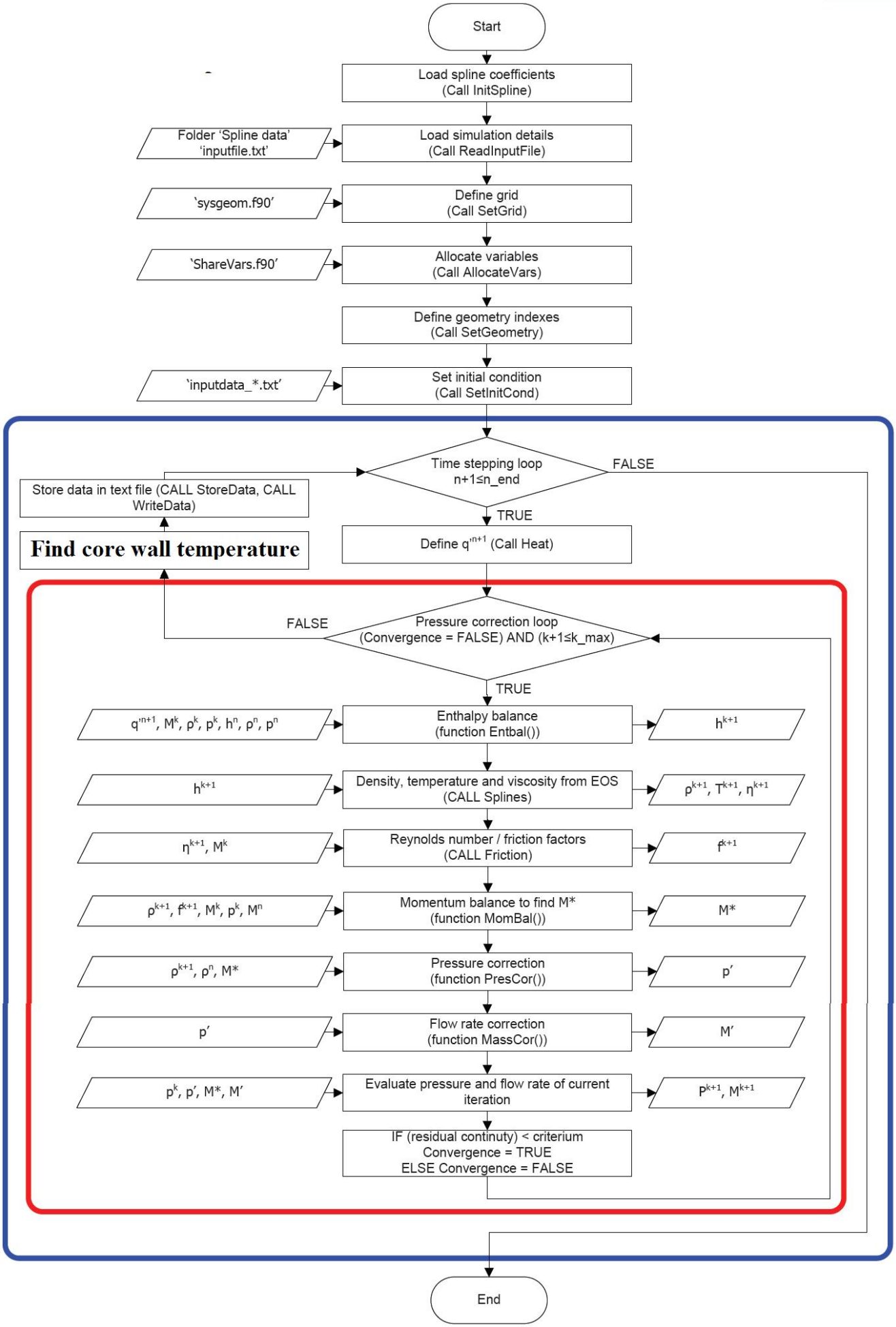

Figure 5.3: Flowchart of the computer model for DeLight. The boxes indicate a major loop in the code. The red box indicates iteration for pressure correction and the blue box indicates time stepping. The wall temperature mechanism is found just outside the red box on the left side. Source: Spoelstra [2012], edited. For a more detailed explanation of the flowchart, see Spoelstra [2012].

6 Benchmarks

What follows in this section is a series of several cases to benchmark the numerical code.

6.1 Steady state benchmarks

The first benchmarks were performed to see if steady state calculations are performed as expected. Three artificial cases were studied: The Nusselt number for internal heat flux was set to zero over the entire core, the Nusselt number for external heat flux was set to zero and the specific heat capacity of the core wall was set to a very large value to mimic infinite heat capacity.

Case I, where the Nusselt number for internal heat flux was set to zero, the enthalpy of the coolant in the core should not rise. This is confirmed by the output of the code, as can be seen in figure 6.2.

Because no heat is transferred to the fluid, all the heat must go to the ambient air. The heat transfer coefficient to the air is quite a bit lower than the heat transfer coefficient to the Freon (see figure 6.1). Because of this the wall temperature of the core must increase quite a bit compared to the standard situation. Figure 6.3 indeed shows this expected trend.

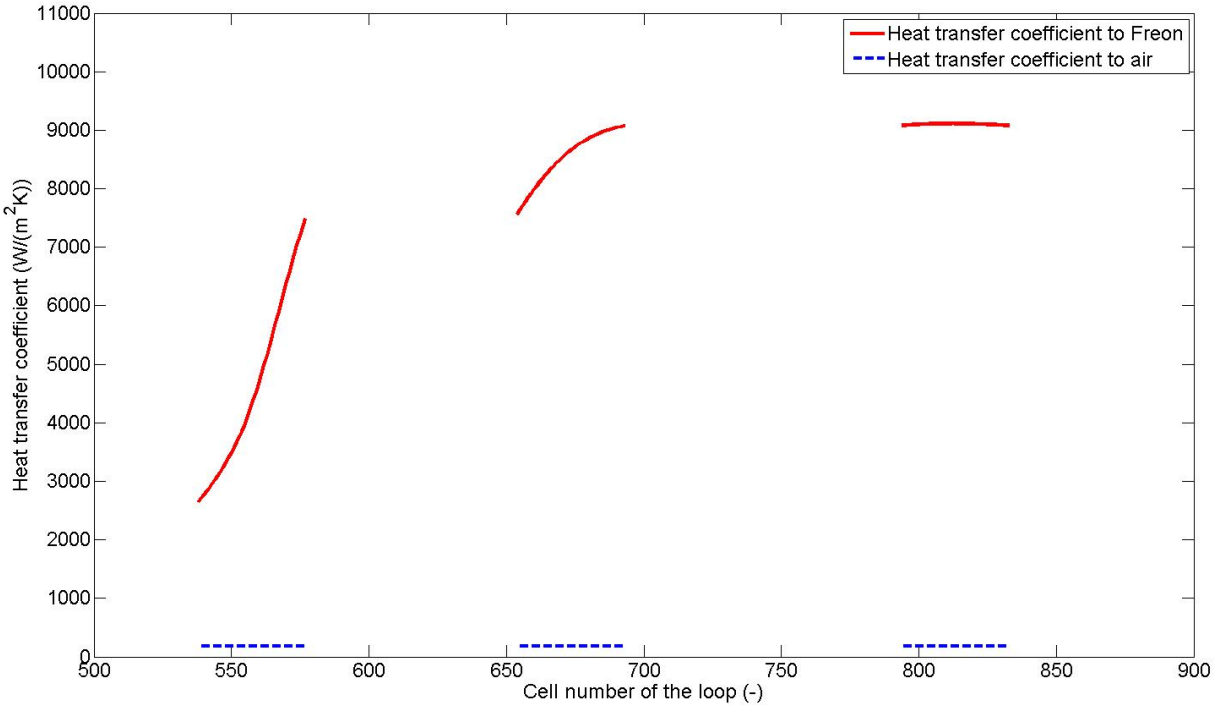

Figure 6.1: Heat transfer coefficient of the different core parts. The red, solid line shows the heat transfer coefficient for heat transfer from the wall to the Freon. The blue, dotted line shows the heat transfer coefficient for heat transfer from the wall to the ambient air. As can be seen, the heat transfer coefficient for internal heat flux is much greater than the heat transfer coefficient for external heat flux. This causes most heat from the wall to go into the Freon, which, obviously, is desired.

For case II, where the Nusselt number for external heat flux was set to zero, it was expected that the enthalpy of the Freon would be overall higher than in the standard situation. All the heat from the core must now go into the Freon. The wall temperature would therefore become slightly higher, just like the enthalpy of the Freon. Figure 6.4 and 6.5 show this trend.

For case III the specific heat capacity was set to a very large value to mimic infinite heat capacity. For this reason, the wall could store a large amount of heat before heating up. Therefore, the operating conditions should never be reached, as the wall cannot become hot enough in time. Also, as the wall is colder than the surroundings, it should withdraw heat from the surroundings instead of losing it. Both results were found when running the code. Over the running time, the wall temperature rose by no more than 1°C.

These three benchmarks neatly behaved as expected and for this reason it is assumed that the code was correctly implemented, at least in the case of a steady state.

6.2 Stability benchmarks

The stability benchmarks are a bit harder to understand than the steady state benchmarks, as these include time dependency as well. There were three types of benchmarks made for the stability calculations: The density of the wall was adjusted, the thickness of the wall was adjusted and the relation for the Nusselt number was changed, case A, B and C respectively.

Case A, changing the wall density, has the same effect as changing the specific heat capacity, as both are the same factor in equation 4.4.2, that is $\rho C_p V$. When the density is increased, it stabilizes the system. This can be understood as follows: When the density is increased, more heat is required to increase the wall temperature. So when a temperature perturbation in the Freon passes by, it will have a smaller effect on the wall temperature. Therefore, the wall temperature will fluctuate less and the fluid temperature oscillation will tend to dampen more easily.

If you look at it the other way around, that is lowering the density, then the wall will need less heat to change temperature. This will cause the wall temperature to fluctuate more when a perturbation passes by. As a limit case, when decreasing the wall density and specific heat capacity to zero, the case of constant heat flux can be approximated, as the temperature difference between wall and fluid becomes approximately constant.

The benchmark was performed on two points of the neutral stability boundary, on the left and right side of the NSB, called the left and right branch. See chapter 7 for an explanation. The case was performed on the left branch at the point where N_{PCH} was 0.4380 and N_{SUB} was 0.4016. On the right branch it was performed where N_{PCH} was 0.7856 and N_{SUB} was 0.3480. The result of this benchmark can be seen in figure 6.6. It shows that the density dependence of the two chosen points indeed behave as expected.

Benchmark B, changing the thickness of the wall, has in principle the same effect as changing the density. The thickness determines the volume of the wall and, therefore, are in the same part of equation 4.4.2 as the density. However, the thickness has an effect on the outer diameter of the system and, therefore, also influences the external heat flux and the Nusselt number for external heat flux (equation 4.4.6). Nevertheless, it was expected that the trend would remain the same. Figure 6.7 shows that this expectation is indeed true.

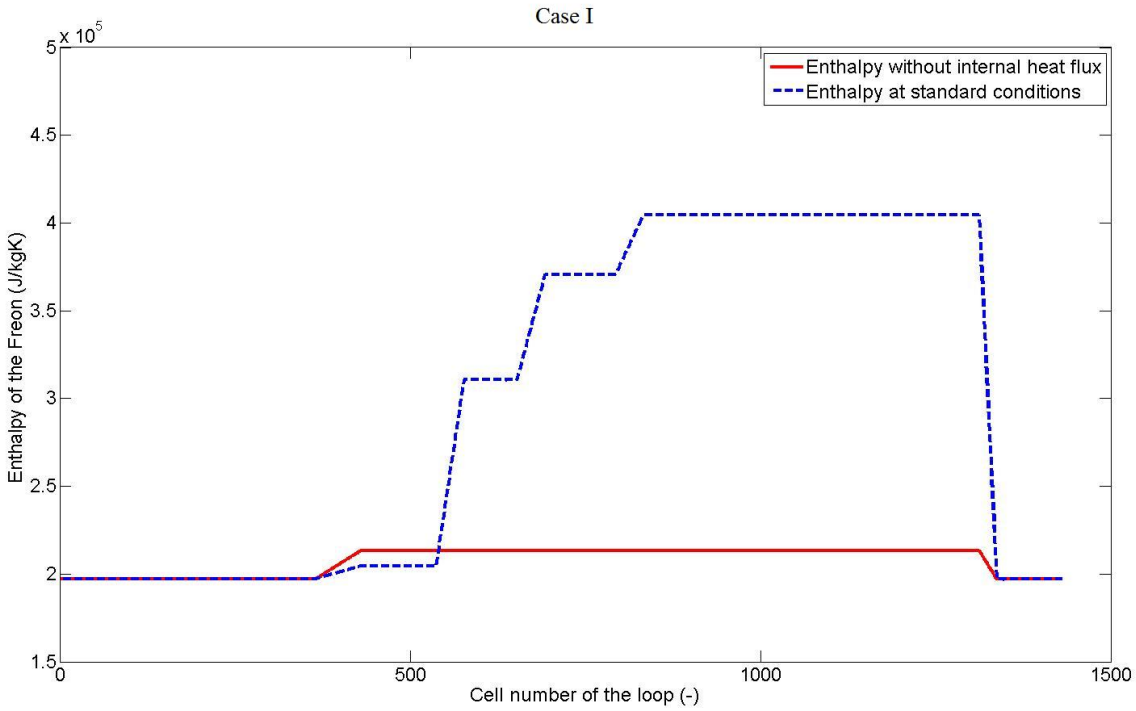

Figure 6.2: Case I. Enthalpy of the Freon through the entire loop. The red, solid line shows the situation where no heat flows into the core. The blue, dotted line shows the situation at standard conditions. The core wall does not heat up the Freon here, as was expected. The small rise before the core indicates the preheater, which was not turned off.

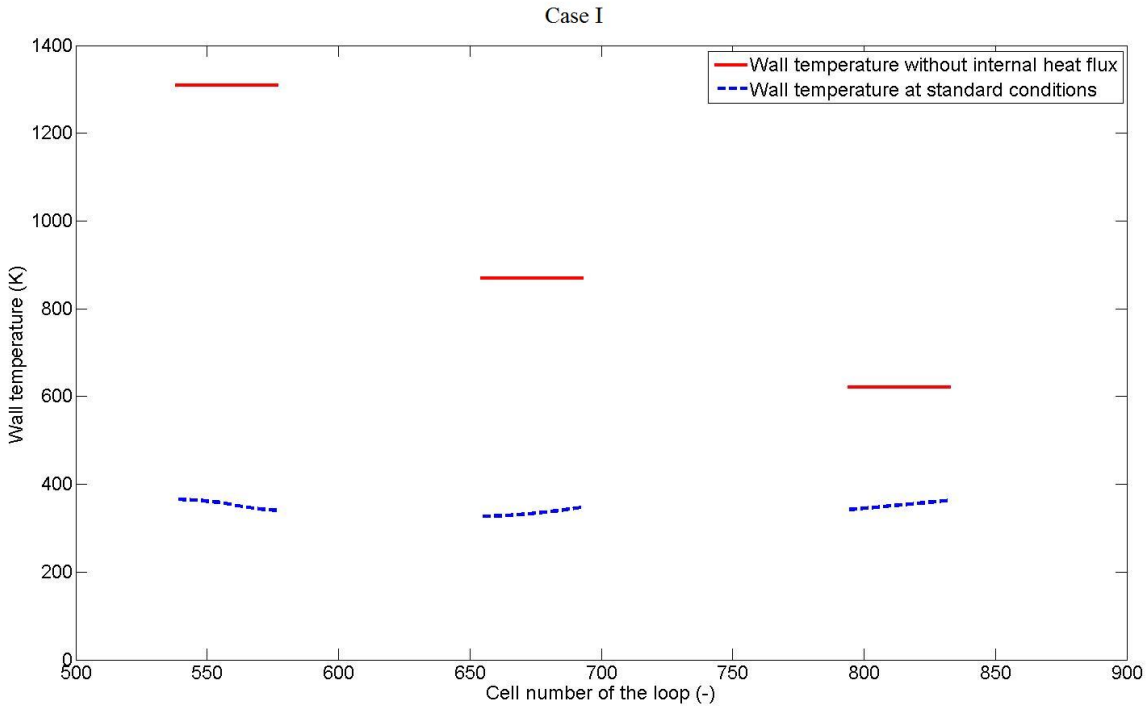

Figure 6.3: Case I. Wall temperature of the different sections of the core. The red, solid line shows the situation without external heat flux. The blue, dotted line shows the situation at standard conditions. The temperature of the wall at non-core parts is left out. Because the wall of the first part of the core, the evaporator, is set to produce the most power, its temperature in this benchmark rises the most.

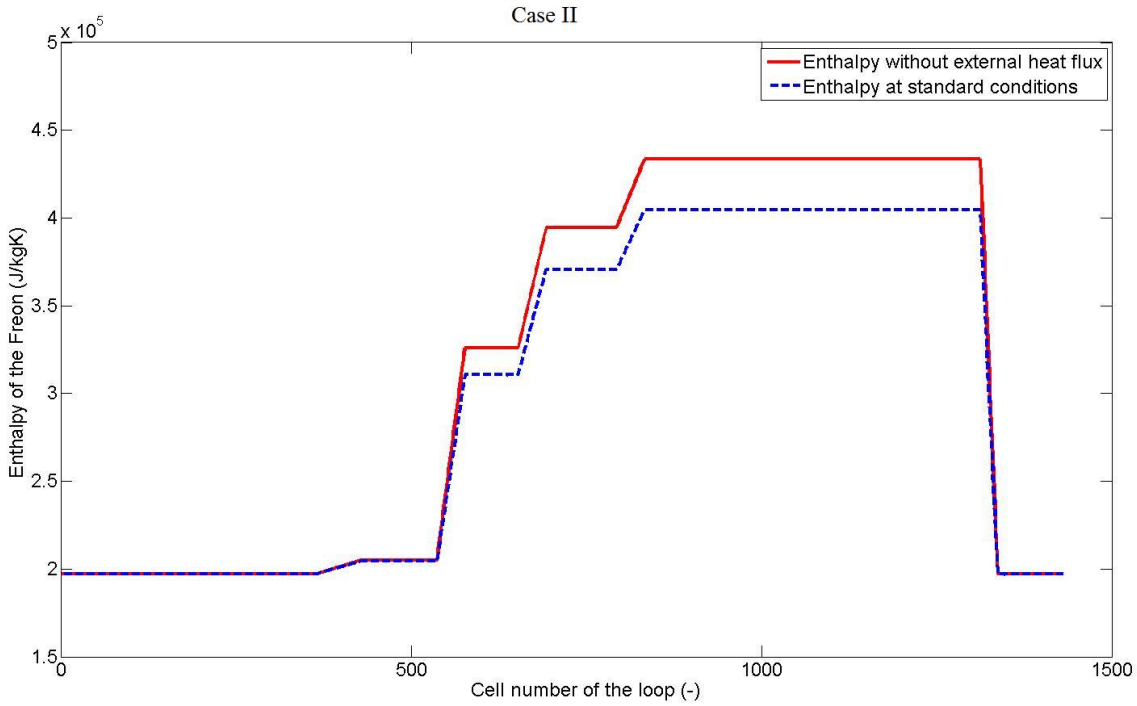

Figure 6.4: Case II. Enthalpy of the Freon through the entire loop. The red, solid line shows the situation without external heat flux. The blue, dotted line shows the situation at standard conditions. The enthalpy of the Freon is higher here than in the standard case, as expected.

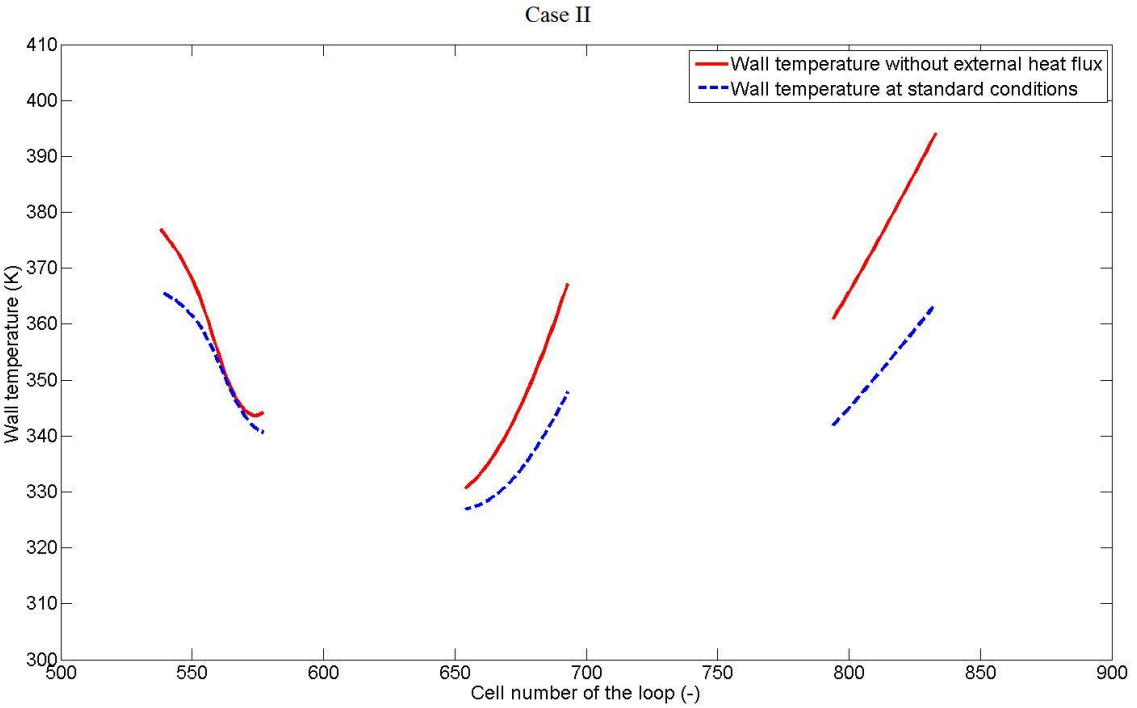

Figure 6.5: Case II. Wall temperature of the different sections of the core. The red, solid line shows the situation without external heat flux. The blue, dotted line shows the situation at standard conditions. The temperature of the wall at non-core parts is left out. The wall temperature is found to be slightly higher in this case than in the original case, as expected.

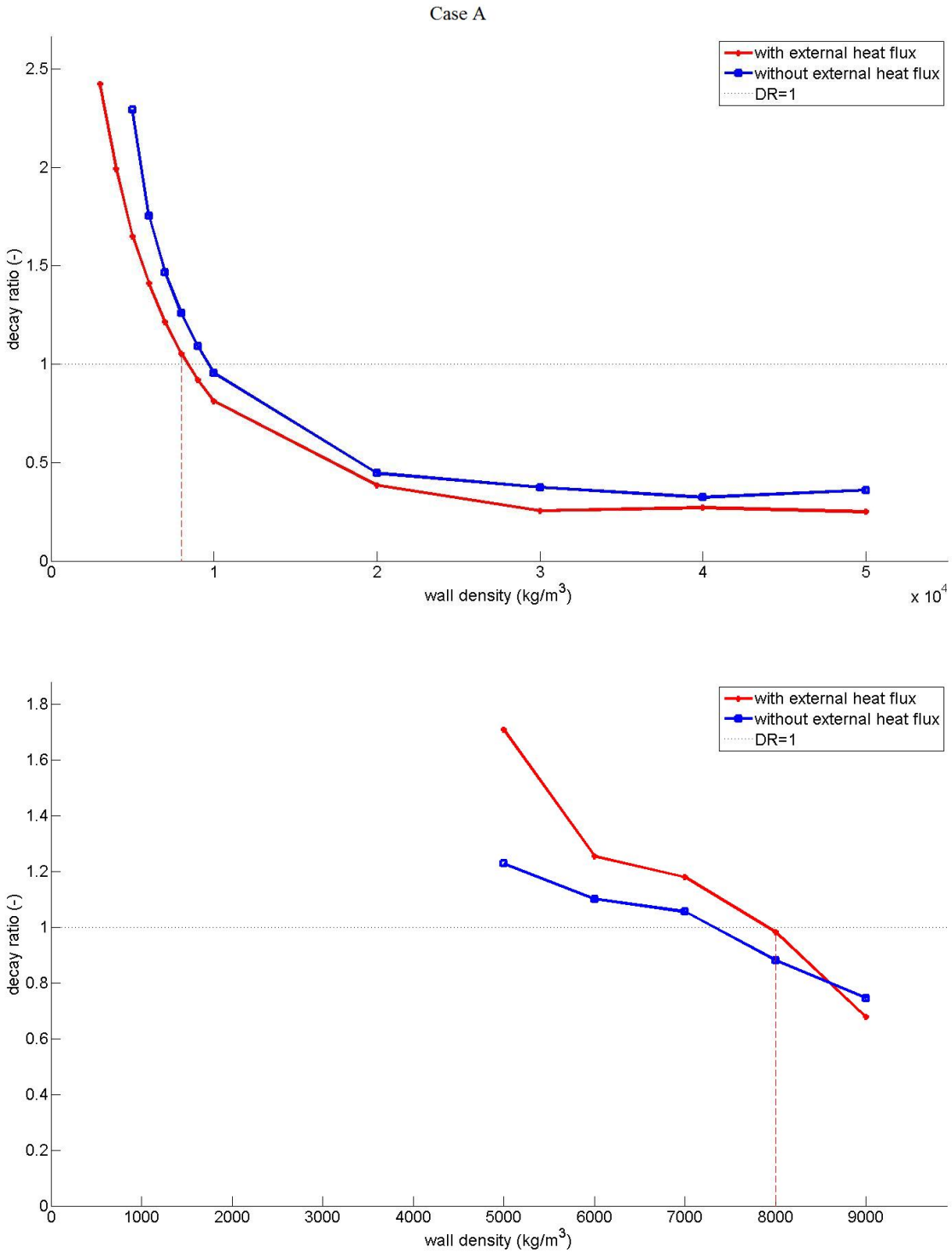

Figure 6.6: Case A. Decay ratio at varying densities at the left branch (top) and the right branch (bottom). The red represents the standard conditions, the blue line is without the external heat flux. The right branch becomes unstable more quickly and when the system becomes too unstable, the code can't solve for it anymore. Therefore there are less points for this case. The original density is 8000 kg/m^3.

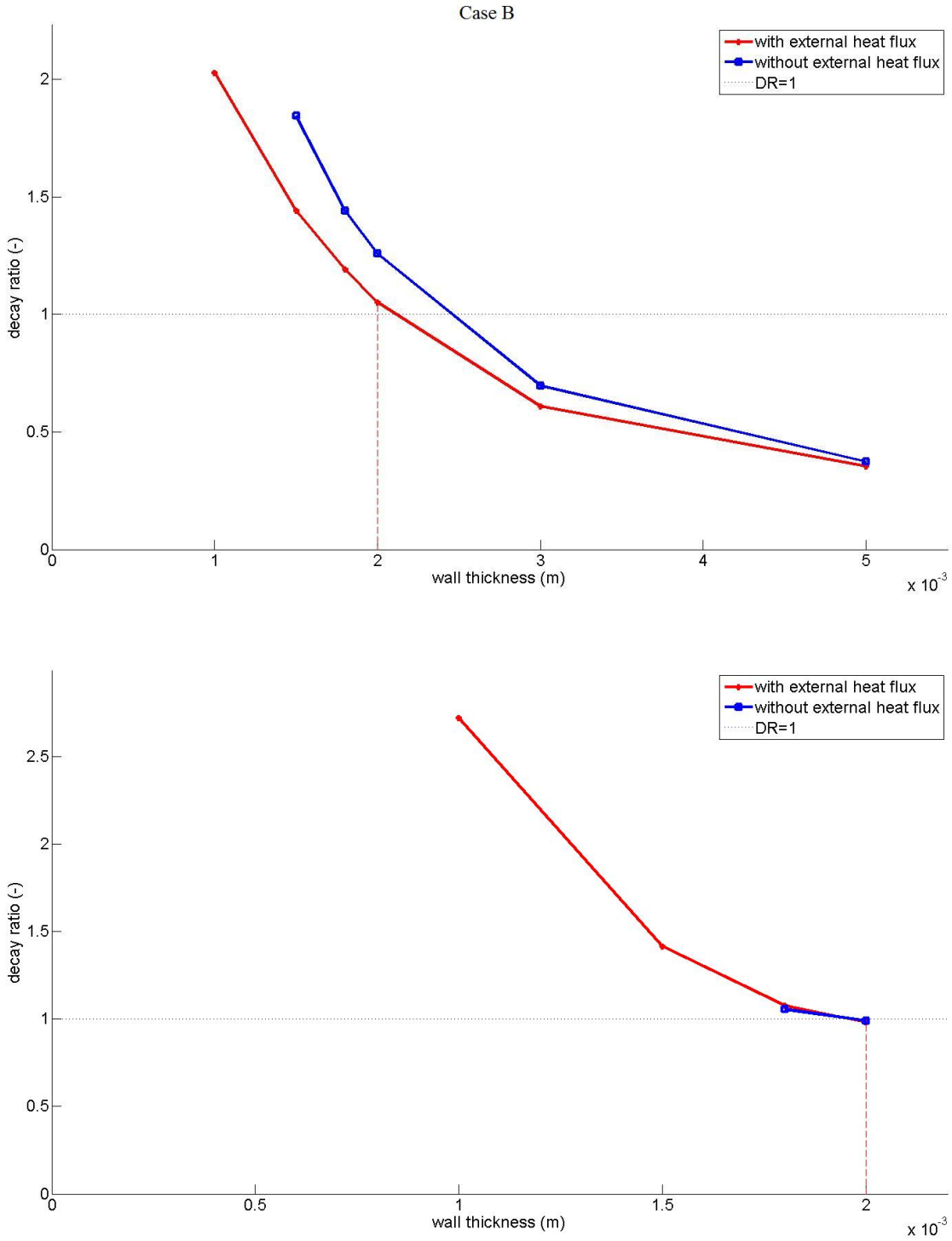

Figure 6.7: Case B. Decay ratio at varying thicknesses at the left branch (top) and the right branch (bottom). The red line represents the standard conditions, the blue line is without external heat flux.The right branch becomes unstable more quickly and when the system becomes too unstable, the code can't solve for it anymore. There are therefore less points for this case. For the bottom blue line only two measurement points were possible and no conclusions could be made for this line. The original wall thickness in the code is $2mm$.

6.3 Approximation of the Spoelstra case

The very last benchmark was made to check if the results Spoelstra [2012] found in his thesis, could be found again by using the new code. For this purpose, the density and specific heat capacity were set to near zero and the Nusselt number for internal heat flux was set to a constant value of 10^4. This value was chosen because it was close to the Nusselt number found by the wall temperature mechanics. The external heat flux was turned off and instead a constant heat flux used by Spoelstra was implemented.

$$Q_{out} = P_{core}\frac{p_{loss}}{100}. \tag{6.3.1}$$

Filling these values into equation 4.4.2;

$$\rho C_p V \frac{dT_{wall}}{dt} = Q - \alpha_{in}\left(T_{wall} - T_{Freon}\right) P_{in} dz - \alpha_{out}\left(T_{wall} - T_{ambient}\right) P_{out} dz,$$

and changing the order of the variables, this equation becomes

$$T_{wall} - T_{Freon} = Q\frac{1 - p_{loss}}{\alpha_{in} P_{in} dz} \tag{6.3.2}$$

All the variables on the right side of the equation are now constant and therefore $T_{wall} - T_{Freon}$ is constant, which causes a constant internal heat flux. As Spoelstra [2012] had constant heat flux, this should be a correct approximation for this case.

The test was ran and the result can be seen in figure 6.8. It shows that the measurement points indeed approximate the neutral stability boundary by Spoelstra [2012] on both branches. The approximation of the right branch show a slight deviation, which can be attributed to the wall temperature mechanics.

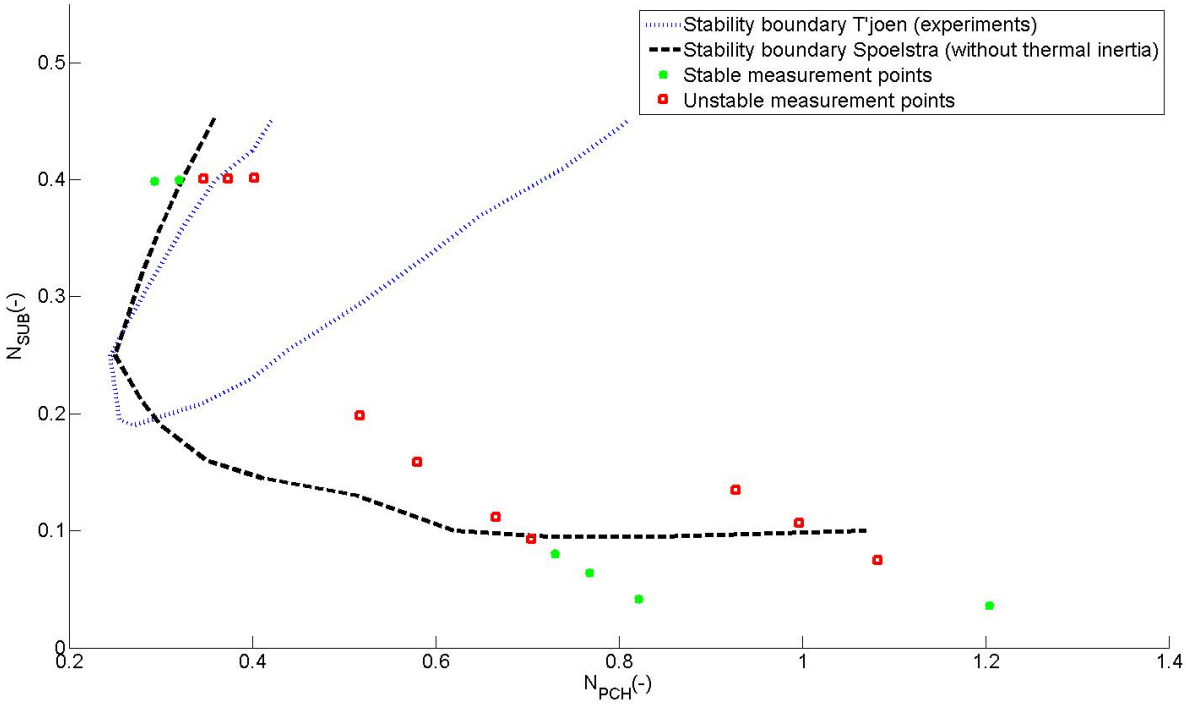

Figure 6.8: Approximation of the Spoelstra case. Three points on the boundary were checked. Red points indicate instable points and green points indicate stable points. As can be seen, both branches are approximated rather well, although a slight deviation is found at the right branch.

7 Results, Nusselt benchmark and discussion

This chapter shows the main results of this thesis and discusses them. It shows the neutral stability boundary calculated including thermal inertia of the wall and compares it to the NSBs found by T'Joen and Rohde [2012] and Spoelstra [2012]. It also shows the result of modeling Nusselt number relations given in section 4.4.3

7.1 NSB including thermal inertia

Figure 7.1 shows the NSBs found by T'Joen and Rohde, Spoelstra and this thesis. Spoelstra found that the left branch matched the left branch of the measurements rather well. The right branch, however, predicted much more unstable behavior.

When looking at the NSB, one can see that the code with wall thermal inertia predicts more stable behavior than Spoelstra's code over the entire given range. While the left branch is too stable now, the right branch approximates the true behavior much better. Even though the NSB still shows a significant deviation from experiments, the trend of the right branch is captured now.

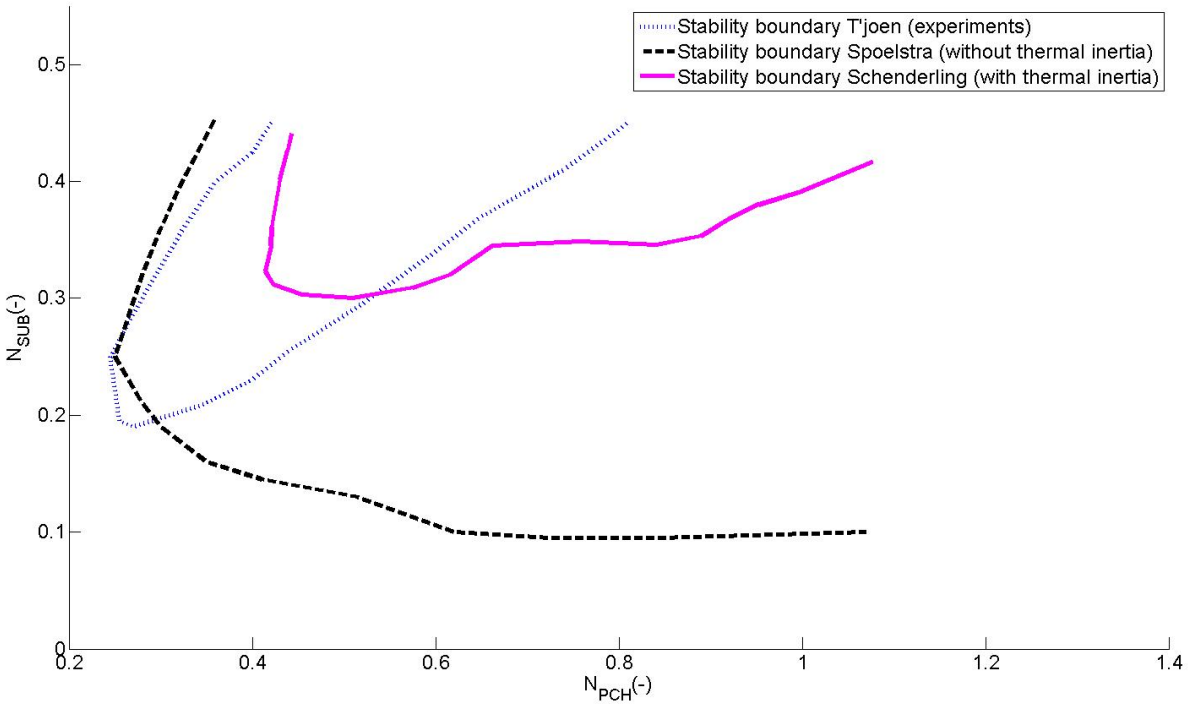

Figure 7.1: Graph of the NSB found by T'Joen, Spoelstra and this thesis on a non-dimensional plane. Everything above the graphs is unstable, while the part under the graphs shows the area where the system is stable

As Spoelstra [2012] indicated in his report, several types of errors are made in the

modeling of the DeLight facility. These include errors in discretization, identifying the physics of the system and errors in the modeling of the identified physics.

- Discretization errors lead to numerical diffusion and stabilize the system. This could explain the behavior of the left branch, but the right branch becomes more unstable than the measurements and thus an explanation of the difference through numerical diffusion seems incorrect or, at least, incomplete.

- Although new physical phenomena were added, a lot of errors in identifying the physics will remain. The phenomena added contained quite a few assumptions. For example, axial heat conduction was not taken into account. Also, the model for the Nusselt number for internal heat transfer was developed for subcritical flow, which means it is probably not accurate for supercritical fluid. The same holds for external heat transfer. On top of all that, the thermal inertia of the wall has only been added in the core section. This means that wall temperature effects in the rest of the system have not been taken into account. This includes the preheater and the heat exchanger, where the thermal inertia were not implemented either.

  Internal Heat transfer is assumed to be instantaneous. In reality it will take some time for the core's heat to reach the bulk of the fluid. Fluctuations in core power caused by the coupling of neutronics and density will affect the internal heat flux a bit later. As changing τ (the time delay between a density change and core power change) was shown by T'Joen and Rohde [2012] to affect stability, this effect could possibly affect the stability as well.

  Core inlet frictions are known to have a stabilizing effect, while core outlet frictions tend to destabilize (Gomez [2009]). Errors in these frictions might have an effect on the NSB. However, steady state analysis by Spoelstra [2012] revealed that steady state calculations were done correctly. Therefore, inlet and outlet frictions are assumed to be correctly implemented.

  Of course, any other unidentified physical phenomena can have an effect on the system. As these are as of yet unknown, it cannot be said if these will further stabilize or destabilize the system.

- Lastly, errors in the modeling of the identified physics have been brought to a minimum by making several benchmarks. These were discussed in chapter 6

7.2 Nusselt benchmark

By changing the models for the Nusselt number, the effect of the Nusselt number can be studied. Changing it does not have an easily predictable effect. As the value of the Nusselt number changes over the core the Nusselt number relations that were used were the Bishop and Jackson relation (Pioro and Mokry [2011]). They can be seen in section 4.4.3. The results of using these relations are in figure 7.2.

It would seem that the result for the figure where the Bishop relation was used, has less points than the figure where the Jackson relation was implemented. However, this was because the steady state procedure did not finish successfully for the right

branch. Thus it cannot be determined if this situation was stable or unstable. This relation seems to cause higher system instability in the model. Using the Jackson relation caused a stabilizing effect on the NSB.

Changing the model for the Nusselt number seems to have a significant effect on the NSB. Therefore, finding the correct model is important to be able to approximate the NSB measured by T'Joen and Rohde [2012].

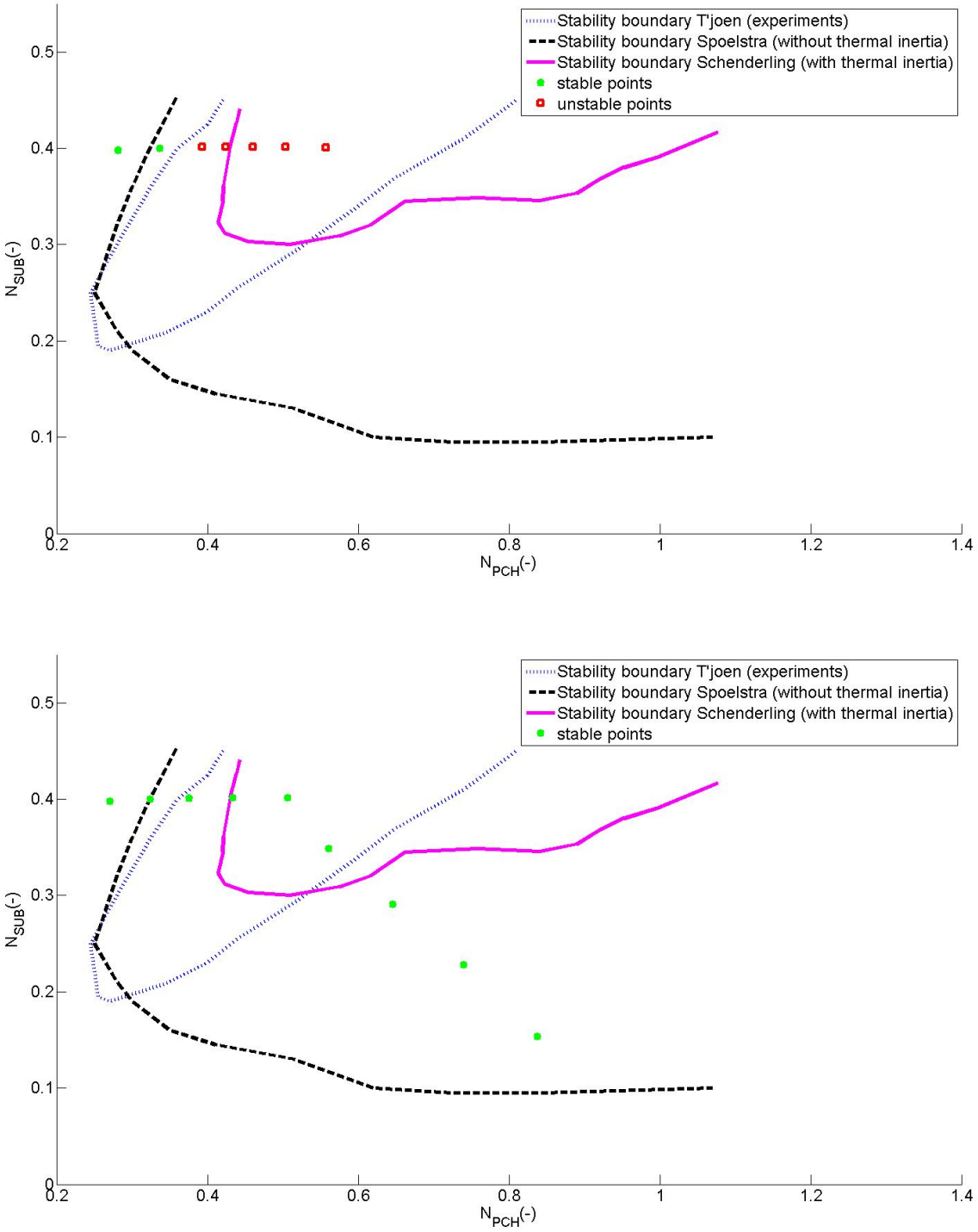

Figure 7.2: The stability points used to find two of the intersections with the Bishop (top) and Jackson(bottom) relation neutral stability boundaries. It can be seen that the Jackson relation has a great effect on stability; no unstable points were found. The code did not finish the steady state calculation successfully when the Bishop relation was used for the right branch. As such, stability points are shown for the left branch only.

8 Conclusions and outlook

In this thesis, an existing computer code to determine the stability of the DeLight (Delft Light water reactor) facility was adjusted to include thermal inertia of the heating walls. The DeLight facility is a model for the High Power Light Water Reactor(HPLWR), a generation IV nuclear reactor. The facility has been used to determine its stability at different operating conditions in terms of power, inlet temperature and friction distribution. The original model was not accurate in predicting this stability; especially at higher power over mass flow it predicted more unstable conditions than were seen in the measurements on the facility. To see if it had a significant effect on stability, thermal inertia was added to the code.

Thermal inertia clearly causes a change in the location of the neutral stability boundary. The system became overall more stable than the code showed without the thermal inertia. At lower power over mass flow it was now too stable, while at higher powers it still predicted too unstable conditions. However, the trend found during the measurements on the DeLight facility was also found in this thesis.

Changing the relation for heat transfer from the core to the coolant had a significant effect on the stability. The original equation, the Dittus-Boelter equation, used in determining the neutral stability boundary was not specifically for supercritical fluids, whereas the benchmark-relations were. Therefore one can conclude that the form of the neutral stability boundary found in this thesis is specific for the Dittus-Boelter equation and not generally applicable. However, it can be concluded that the added code, and thus the core mechanics, has a significant effect on the neutral stability boundary of the system.

Several simplifications and assumptions were made in this thesis and should be further investigated. First of all, a correct model for the Nusselt number for heat going from the wall to the coolant should be found, as it has a significant effect on the neutral stability boundary. This is currently under investigation in the section of NERA in Delft. Secondly, axial and radial heat transfer of the wall from one node to another was left out. This should be implemented in later work. Thirdly, In terms of thermal inertia, more than just the core has an effect on the stability of the system. Thermal inertia should be added in other parts of the coolant loop as well. Lastly, It could be important to search for other possible effects that might influence the stability, such as the position of the buffer vessel or friction distributions, especially at the in- and outlet of the core.

References

H. Bijl. *Computation of flow at all speeds with a staggered scheme*. PhD thesis, Delft University of Technology, 1999.

J. Boure, A. Bergles, and L. S.Tong. Review of two-phase flow instability. *Nuclear Engineering and Design*, 25:165–192, 1973.

K. Fukuda and T. Kobori. Classification of two-phase flow instability by density wave oscillation model. *Journal of Nuclear Science and Technology*, 16(2):95–108, 1979.

T. Ortega Gomez. Stability analysis of the high performance light water reactor, 2009.

L. P. B. M. Janssen and M. M. C. G. Warmoeskerken. *Transport phenomena data companion*. VSSD, 1987.

F. A. L. Kam. Development of a one-dimensional computer model for the stability analysis of a natural circulation supercritical water reactor, 2011.

H. K. Koopman. Development of the STEALTH-code and investigation of the effects of feedwater sparger positioning on the thermal-hydraulic stability of natural circulation boiling water reactors, 2008.

NIST. Reference Fluid Thermodynamic and Transport Properties Database.

OECD. GEN-IV website SCWR technical section, July 2013. URL `http://www.gen-4.org/Technology/systems/scwr.htm`.

S. V. Patankar. *Numerical heat transfer and fluid flow*. Hemisphere publishing corporation, 1980.

I. Pioro and S. Mokry. Heat transfer to fluids at supercritical pressures. 2011.

M. Rohde, C. P. Marcel, C. T'Joen, A. G. Class, and T. H. J. J. van der Hagen. Downscaling a supercritical water loop for experimental studies on system stability. *Nuclear Engineering and Design*, 54:65–74, 2011.

T. Schulenberg, J. Starflinger, and J. Heinecke. Three pass core design proposal for a high performance light water reactor. *Progress in nuclear energy*, 50:526–531, 2008.

J. Spoelstra. Numerical stability analysis of natural circulation driven supercritical water reactors, 2012.

C. T'Joen and M. Rohde. Experimental study of the coupled thermo-hydraulic-neutronic stability of a natural circulation HPLWR. *Nuclear Engineering and Design*, 242:221–232, 2012.

C. T'Joen, L. Gilli, and M. Rohde. Sensitivity analysis of numerically determined linear stability boundaries of a supercritical heated channel. *Nuclear Engineering and Design*, 241:3879–3889, 2011.

C. T'Joen, M. Rohde, and M. De Paepe. Linear stability analysis of a supercritical loop. 9^{th} *International conference on heat transfer, fluid mechanics and thermodynamics*, 2012.